REPORT DOCUMENTATION PAGE

Form Approved
OMB No. 0704-0188

1. AGENCY USE ONLY (Leave blank)	2. REPORT DATE Dec 94	3. REPORT TYPE AND DATES COVERED

4. TITLE AND SUBTITLE
The effect of Viscous Attenuation on Shock Tube Performance

5. FUNDING NUMBERS

6. AUTHOR(S)

Nick Roger McKenzie

7. PERFORMING ORGANIZATION NAME(S) AND ADDRESS(ES)

AFIT Students Attending:

Univ of Tennessee

8. PERFORMING ORGANIZATION REPORT NUMBER
AFIT/CI/CIA

94-168

9. SPONSORING/MONITORING AGENCY NAME(S) AND ADDRESS(ES)

DEPARTNEMT OF THE AIR FORCE
AFIT/CI
2950 P STREET, BDLG 125
WRIGHT-PATTERSON AFB OH 45433-7765

DTIC
ELECTE
JAN 18 1995
S G D

10. SPONSORING/MONITORING AGENCY REPORT NUMBER

11. SUPPLEMENTARY NOTES

12a. DISTRIBUTION/AVAILABILITY STATEMENT

Approved for Public Release IAW AFR 190-1
Distribution Unlimited
BRIAN D. GAUTHIER, MSgt, USAF
Chief Administration

12b. DISTRIBUTION CODE

13. ABSTRACT (Maximum 200 words)

19950117 007

DTIC QUALITY INSPECTED 3

14. SUBJECT TERMS		15. NUMBER OF PAGES 59
		16. PRICE CODE

17. SECURITY CLASSIFICATION OF REPORT	18. SECURITY CLASSIFICATION OF THIS PAGE	19. SECURITY CLASSIFICATION OF ABSTRACT	20. LIMITATION OF ABSTRACT

ABSTRACT

Shock wave attenuation affects experimental results by reducing the shock velocity as it travels down the shock tube. Until recently, attenuation has not been readily predictable with accuracy and was simply accepted during the experimental process. A mass loss theory was developed by Dr. Harold Mirels which accounted for the shock wave attenuation by considering the formed boundary layer due to the passage of a shock wave. The purpose of this thesis is to develop a computer code, which would apply Mirels' theory to a prediction model, and validate the results with acoustic theory and Mirels' data. It will then be used to determine an accurate shock velocity for an additional shock tube. The computer results will be proven to match the experimental data well. However, additional corrections involving friction, heating, and real gas effects are needed to produce excellent results. It will also be discovered that the mass loss correction results are a significant part of the total shock wave attenuation.

BIBLIOGRAPHY

Anderson, John D., Jr. <u>Modern Compressible Flow With Historical Perspective</u>. 2nd ed. New York: McGraw-Hill, 1990. 207-214.

Campbell, John W. "Enhanced Vision Systems." Thesis University of Tennessee Space Institute 1994.

Glass, I. I. "Appraisal of UTIAS Implosion-Driven Hypervelocity Launchers and Shock Tubes." <u>Progress In Aerospace Sciences</u>. Ed. D. Kuchemann. vol. 13. Oxford: Pergamon Press, 1972.

Glass, I. I. "Beyond Three Decades of Continuous Research at UTIAS on Shock Tubes and Waves." AFOSR-TR-81-0783 University of Toronto, 1981. 1-12.

Gottlieb, J. J., and Glass, I. I. "Recent Developments In Sonic-Boom Simulation Using Shock Tubes." <u>Recent Developments In Shock Tube Research: Proceedings of the Ninth International Shock Tube Symposium</u>. Stanford University, 1973.

Maus, J. R. "A Mathematical Model for the G-Range Impulse Facility." AEDC-TMR-91-V10 October, 1991.

Maus, J. R., Laster, M. L., and Hornung, H. G. "The G-Range Impulse Facility - A High Performance Free-Piston Shock Tunnel." AIAA Paper 92-3946 July, 1992.

Maus, J. R. Personal communication between May and December, 1994.

Mirels, H. "Attenuation In a Shock Tube Due to Unsteady-Boundary-Layer Action." NACA Report 1333 April,1956 a.

Mirels, H. "Boundary Layer Behind Shock or Thin Expansion Wave Moving Into Stationary Fluid." NACA TN 3712 May, 1956 b.

Mirels, H. "Shock Tube Test Time Limitation Due to Turbulent-Wall Boundary Layer." AIAA J. 2, 84 1964.

Smith, M. S. Personal communication concerning the diagnostic development shock tube at AEDC August, 1994.

Trimpi, R. L., and Cohen, N. B. "A Theory For Predicting the Flow of Real Gases in Shock Tubes With Experimental Verification." NACA TN 3375 March, 1955.

Wright, J. K. Shock Tubes. New York: John Wiley & Sons, Inc., 1961. 1-2.

THE EFFECT OF VISCOUS ATTENUATION ON SHOCK TUBE

PERFORMANCE

A Thesis

Presented for the

Master of Science

Degree

The University of Tennessee, Knoxville

Nick Roger McKenzie

December 1994

DEDICATION

This thesis is dedicated

to my wife,

Melissa Anne McKenzie

my parents, Roy and Alberta

and my brother, Matt.

Their love and unending support have contributed

to all of my successes and assisted recovery

from all of my failures.

ACKNOWLEDGMENTS

I would also like to thank my wife, Melissa, for her patience and understanding during many frustrating afternoons and long nights. Her support has been paramount. Finally, I would like to thank God for answering my prayers.

ABSTRACT

Shock wave attenuation affects experimental results by reducing the shock velocity as it travels down the shock tube. Until recently, attenuation has not been readily predictable with accuracy and was simply accepted during the experimental process. A mass loss theory was developed by Dr. Harold Mirels which accounted for the shock wave attenuation by considering the formed boundary layer due to the passage of a shock wave. The purpose of this thesis is to develop a computer code, which would apply Mirels' theory to a prediction model, and validate the results with acoustic theory and Mirels' data. It will then be used to determine an accurate shock velocity for an additional shock tube. The computer results will be proven to match the experimental data well. However, additional corrections involving friction, heating, and real gas effects are needed to produce excellent results. It will also be discovered that the mass loss correction results are a significant part of the total shock wave attenuation.

TABLE OF CONTENTS

LIST OF FIGURES

LIST OF SYMBOLS

A   area

a   speed of sound

b   calculation coefficient (Equation 3.17)

c   calculation coefficient (Equation 3.17)

C_p specific heat at constant pressure

C_v specific heat at constant volume

DPF   pressure drop term due to friction forces

E   energy

e   specific internal energy

h   enthalpy

I_N integral defined in Equation 3.21

J   mass point counter

M   Mach number

M_a integrand term (Chapter 4)

m   mass

$\dot{m}$ mass flow

N	cycle indentifier
P	pressure
Pr	Prandtl number
P_2	pressure behind shock wave for the classical theory
$P_{2,d}$	pressure behind shock wave for the attenuated shock wave
Q	dissipation factor
q	rate of heat transfer in y-direction
R	gas constant
Re	Reynolds number
T	absolute static temperature
T_m	absolute mean temperature
T_r	absolute wall surface static temperature for zero heat transfer
t	time
U_s	oncoming flow velocity for a shock fixed coordinate system
u	velocity term
u_e	velocity behind shock wave for a shock fixed coordinate system
u_p	fluid velocity behind moving shock wave
u_w	wall velocity for shock fixed coordinate system

V	volume (Figure 7 and Equations 4.4 and 4.5)
v	specific volume (Chapter 2, Equation 2.4)
v	normal velocity
W	moving shock wave velocity
δ	fluid velocity boundary layer thickness
δ	fluid velocity boundary layer thickness - Pohlhausen viewpoint
δ^*	fluid boundary layer displacement thickness
ϕ	function (Equation 3.26)
γ	ratio of specific heats
μ	coefficient of viscosity
ρ	density
τ_w	local shear stress exerted by fluid on wall
ξ	integration variable for x
θ	fluid boundary layer momentum thickness
ζ	similarity parameter

Subscripts

e	flow external to fluid boundary layer

m   quantity evaluated at T_m

r   recovery

s   shock

w   quantity evaluated just above wall surface

CHAPTER I

INTRODUCTION

INTRODUCTION

Since its invention in the early 1900's, the shock tube has provided a simple and inexpensive high speed flow phenomena testing facility. Its versatility has earned itself a regime of its own in the world of aerospace testing. Because of its wide spread use, a large interest in the shock tube technology has ensued, concerning the characteristics and performance of the shock tube. These interests range from attenuation to flow zones.

Early on in shock tube research, the attenuation phenomenon interfered with accurate shock wave velocity predictions. Initial investigations were accomplished, but reliable, conclusive results were never realized. In the 1950's Dr. Harold Mirels arrived at a theory which explained shock wave attenuation due to the viscous wall boundary layer interaction produced by the passage of the shock wave. His theory dealt with mass accountability in the shock tube system. A mass transfer into the boundary

1

layer was causing perturbations, resulting in the attenuation of the shock wave (Mirels, 1956a). Building on the theory, he developed a set of equations which addressed the problem of attenuation in several different cases.

Despite these developments, most laboratories simply lived with the attenuation problem. Tedious calculations producing accurate results were inefficient when estimates provided enough information. Since shock tubes were small and simple to operate at the time, multiple runs to achieve a single test condition were not unmanageable. The advent of larger and more complicated shock tubes increased the demand for better predictions. The computer age allowed for better measurement techniques. More accuracy in measurements demanded more accuracy in predictions. With this in mind, the purpose of this thesis becomes apparent.

PURPOSE

The purpose of this thesis is to provided a computer model of shock tube flow characteristics while accounting for the shock wave attenuation based on Mirels theory. Shock wave attenuation is made up of several

aspects including: friction, heating, real gas effects, and Mirels' mass loss theory. This study will focus on the mass loss due to a turbulent wall boundary layer interaction. The code is intended to be as versatile as the shock tube. It should be applicable to all shock tube configurations and produce an accurate prediction of the shock wave velocity, in addition to other important shock tube parameters.

CHAPTER II

SHOCK TUBES

INTRODUCTION

A shock tube can be characterized as a simple machine which generates complex phenomena. It consists, basically, of a rigid tube divided into two sections. These sections are separated by a gas-tight diaphragm which is mounted normal to the axis. Initially, a significant pressure difference exists between the two sections. The high pressure section is called the compression chamber while the low pressure section is known as the expansion chamber. At time zero, when the diaphragm is ruptured, the pressure begins to equalize in the form of a shock wave moving into the expansion chamber and a rarefaction wave moving into the compression chamber (e.g.: Wright, 1961). Figure 1 is a simple shock tube schematic, where P_4 is the high pressure in the expansion chamber and P_1 is the low pressure in the compression chamber. For the remainder of this text, the expansion chamber will be noted as the driver section, while the compression
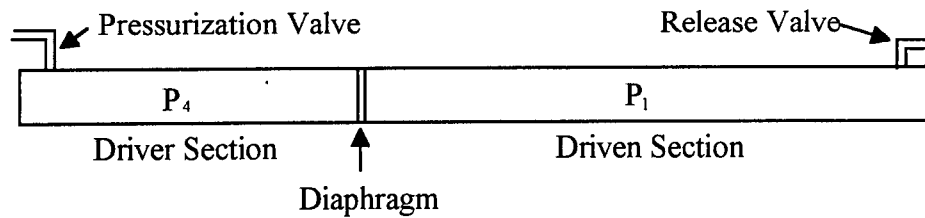
Figure 1. Simple shock tube

chamber will be referred to as the driven section. After the diaphragm has been ruptured, the shock wave will move from left to right, starting at the diaphragm. An induced air flow will follow the shock wave. An expansion wave will move from right to left, beginning at the diaphragm. There are several different versions and modifications which can be made to the simple shock tube. Only those relevant to this text will be mentioned here.

HISTORY

The shock tube appeared just prior to the 1900's, when Vielle proved that the shock wave moved faster than the speed of sound down the tube. After this, the shock tube was dormant until the advent of World War II. Reynolds used the shock tube in 1943 to calibrate piezoelectric pressure gauges used in blast wave measurements. In 1945, a method for photographing the position of a shock front was perfected and a detailed

study of reflected waves was initiated by L. G. Smith (Wright, 1961). After the war, shock tubes seemed to become an institution of their own. W. Bleakney developed a way to determine pressure data for the diffraction of a shock wave around obstacles. He used a Mach Zehnder interferometer to find the quantitative density which was then used to find the pressure (Wright, 1961). From 1948 to 1958, shock tube studies concentrated on one-dimensional flows induced by shock and rarefaction waves while a secondary arena involved contact surface interactions (Glass, 1981). This decade also saw the advent of many problems with shock tube experiments. These phenomena hindered ideal test conditions and still present problems today. The first apparent problem was the diaphragm burst. The ruptured diaphragm's irregular shape occupied some of the tube's cross-sectional area. In addition, barbs from the diaphragm induced turbulence in flow through the ruptured diaphragm, as shown in Figure 2. Because of this, flow quality was degraded by the burst diaphragm. The next problem identified dealt with the shock velocity. It was found that as the shock moved down the tube, its velocity and Mach number decreased. Studies showed that the rate reduction was due to attenuation of the shock wave. Interaction of the side
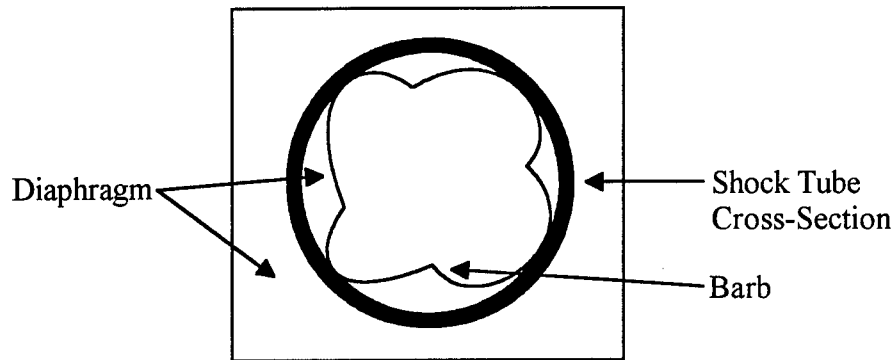
Figure 2. Cross-sectional sketch of burst diaphragm in shock tube

wall boundary layer induced by the shock wave was responsible for the attenuation and an acceleration of the contact surface. This phenomena affected characteristics of each run and shortened the usable test time. An additional problem caused by boundary layer interactions was flow gradients in the driven section (Glass, 1981). The attenuation due to the boundary layer interaction is the reason for this thesis.

Despite these shortcomings, the shock tube had the advantage of being versatile and relatively inexpensive. Its appearance in university, commercial, and government facilities sparked the introduction of some useful modifications. These included: shock tunnels, multidiaphragm shock tubes, and expansion tunnels (e.g.: Glass, 1981). The Engineering Research Institute, at the University of Michigan used a shock tube to drive an

intermittent wind tunnel (Wright, 1961). These hybrids allowed the shock tube to secure a strong foothold in the future of aerospace studies.

Work at the University of Toronto, Institute for Aerospace Studies, (UTIAS), focused on prominent characteristics of the shock tube. One of these characteristics was wave interactions. Shock wave refractions at a contact surface and through a gas layer were examined. It was found that special refracted shock waves would reflect only Mach wave from a contact surface. The result was "the reflected shock wave, tailored-interface, shock-tunnel operation, thereby providing a constant-pressure high-enthalpy reservoir of gas for expansion through supersonic or hypersonic nozzles" (Glass, 1981). Continuing experiments dealt with protective gas barriers for attenuating blast waves, one shock wave overtaking another, and speed of sound measurements for different gases. Shock wave/shock wave and shock wave/rarefaction wave collisions were also investigated. It was found that very high temperatures could be reached through the collision of two shock waves of equal strength. The last important point in this wave of experiments at UTIAS was the finding that strong shock wave predictions had to include real gas effects in their calculations in order to match the

experimental results. This was probably no surprise, since strong shock waves will induce high enthalpy flows. However, it did imply that one-dimensional shock theory was, at best, and estimate in most experiments involving shock tubes.

In the 1960's, the shock tube applied itself outside the world of aerodynamics by producing industrial grade diamonds from graphite. The pressures generated to form the diamonds were measured in the megabar range, while temperatures soared above the million degree mark. Although diamond sizes were small, (10-20 micrometers), several companies, including 3M Canada Ltd., continued the study with large success. This configuration also developed fusion plasmas in deuterium (Glass, 1981). Another use of the shock tube outside the aerospace industry is the development of high power gasdynamic and chemical lasers (Anderson, 1990).

An example of a hypersonic conditions simulator is the G-Range Impulse Facility at the Arnold Engineering and Development Center (AEDC). This facility doubles as a high performance free piston shock tunnel and a two-stage light gas gun. Predictions for the shock tunnel include

stagnation pressures of 10,000 atm. and enthalpies of 20 MJ/kg (Maus, Laster, and Hornung, 1992). Figure 3 shows the launcher and shock tunnel configurations. The shock tunnel offers the advantage of a recoverable model while still maintaining high Mach numbers and temperatures. These facilities represent the latest in hypersonic testing mechanisms.

The shock tube has become, and will probably remain a mainstay of the aerospace testing community. It is an inexpensive resource which can be found throughout the world in government, commercial, and university laboratories. Because of its adaptability and versatility, it provides a variety of test conditions, including those conditions which cannot be duplicated by any other type of facility. Derivatives of the shock tube technology have provided results in areas which were previously unsolved. The shock tube has even expanded its usefulness into other industries. Despite reductions in funding, advances in shock tubes and testing techniques continue to set the stage for more practical results and widespread applications.
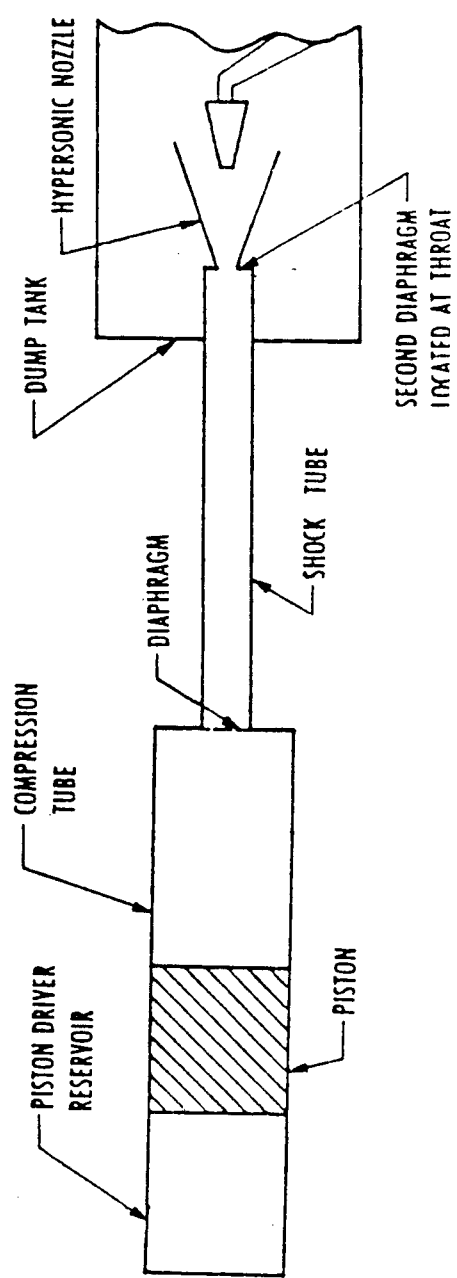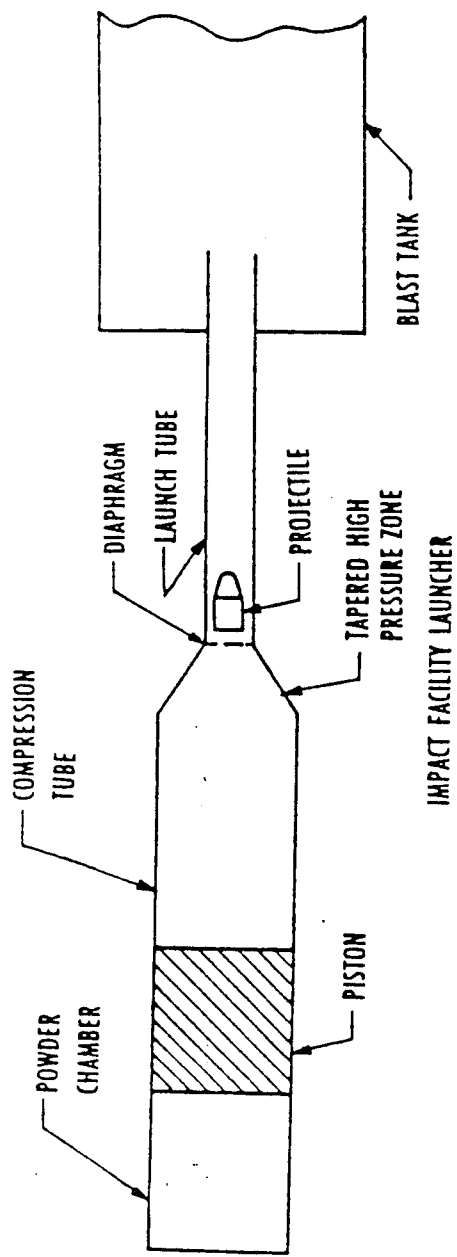
Figure 3. Impulse Facility Launcher and shock tunnel at AEDC
(Maus, Laster, and Hornung)

11

SHOCK TUBE THEORY

The basis for shock tube theory is the assumptions and derivations for a moving normal shock wave. In certain cases, including this thesis, the expansion wave is irrelevant because testing is completed by the time the expansion wave has interfered. Therefore, the expansion wave process is excluded from the derivations of moving normal shock wave equations for shock tubes. Derivation of these equations can be found in Anderson's *Modern Compressible Flow*, and begins with the following forms of the continuity, momentum, and energy equations for a shock fixed coordinate system:

$$\rho_1 u_1 = \rho_2 u_2 \tag{2.1}$$

$$P_1 + \rho_1 u_1^2 = P_2 + \rho_2 u_2^2 \tag{2.2}$$

$$h_1 + u_1^2/2 = h_2 + u_2^2/2 \tag{2.3}$$

where u_1 is the velocity of the gas ahead of the shock wave and u_2 is the velocity of the gas behind the shock wave. Both velocities are relative to the shock wave (Anderson, 1990). Substituting W for u_1 and W-u_p for u_2 yields the following set of equations:

$$e_2 - e_1 = (v_1 - v_2)(p_1 + p_2)/2 \tag{2.4}$$

12

Equation 2.4 is the *Hugoniot equation,* which is the same for moving and stationary shocks. Here $v = RT/p$ and $e = c_v T$. The rest of the relationships follow for the moving shock wave in laboratory coordinates:

$$M_s = W/a_1 \qquad (2.5)$$

$$\frac{T_2}{T_1} = \frac{p_2}{p_1}\left(\frac{\frac{\gamma+1}{\gamma-1}+\frac{p_2}{p_1}}{1+\frac{\gamma+1}{\gamma-1}\frac{p_2}{p_1}}\right) \qquad (2.6)$$

$$\frac{\rho_2}{\rho_1} = \frac{1+\frac{\gamma+1}{\gamma-1}\frac{p_2}{p_1}}{\frac{\gamma+1}{\gamma-1}+\frac{p_2}{p_1}} \qquad (2.7)$$

$$u_p = \frac{a_1}{\gamma}\left(\frac{p_2}{p_1}\right)\sqrt{\frac{\frac{2\gamma}{\gamma+1}}{\frac{p_2}{p_1}+\frac{\gamma-1}{\gamma+1}}} \qquad (2.8)$$

$$W = a_1\sqrt{\frac{\gamma+1}{\gamma-1}\left(\frac{p_2}{p_1}-1\right)+1} \qquad (2.9)$$

where the specific heat ratio is: $\gamma = C_p/C_v$. Figure 4 is reproduced from Anderson and shows the one-dimensional theoretical pressure distribution throughout a shock tube. The shock Mach number, M_s, is found by dividing W by a_1. The shock tube is labeled with notation corresponding to the above equations. The shock wave and contact surface move from left to right while
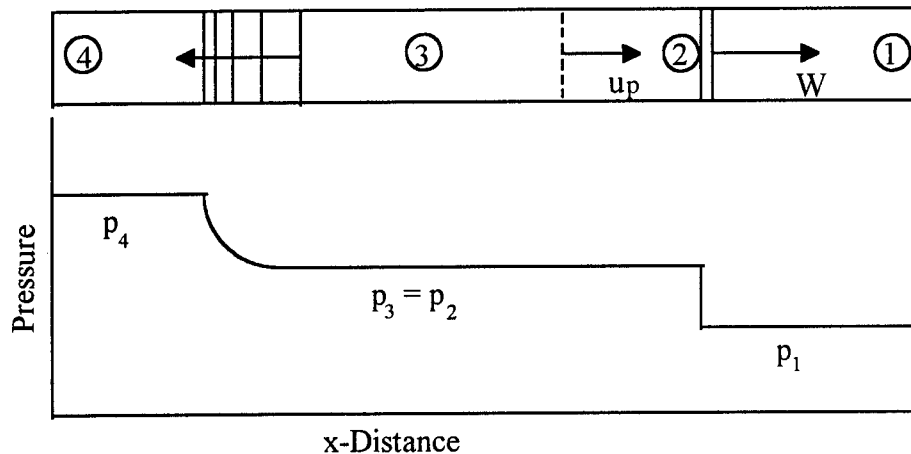
13

Figure 4. Shock tube flow with theoretical pressure distribution after diaphragm burst (Anderson, 1990)

the expansion wave moves from right to left. Regions 1 and 4 are intentionally identified because they will remain in their initial state throughout the test. Region 2 consists of the driven gas after shock wave interaction. Region 3 is the most complicated region since it includes both the driver and driven gases, should they be different, and has interacted with the shock wave and the contact surface. For most testing and computations however, this region is ignored due to its small role in the shock wave propagation.

An interesting note concerning the flow velocity behind the shock wave is its limiting value. If a calorically perfect gas is assumed with a γ of 1.4 and a pressure ratio approaching infinity, the maximum Mach number of

the flow behind the shock wave is 1.89 (Anderson, 1990). This can be confirmed by taking the limit of the equation for the ratio of u_p/a_2 as shown in equation 7.19 of Anderson. This unsteady flow theory forms the basis for shock tube analysis and calculations.

CHAPTER III

MIRELS' SHOCK WAVE ATTENUATION THEORY

INTRODUCTION

One-dimensional shock tube theory gives a good estimate for the shock Mach number in a shock tube. For low Mach numbers (M < 1.5 approximately), the Mach number estimate may even be considered accurate. According to classical theory, this shock Mach number is considered a constant from the diaphragm to the end of the driven section for a constant area tube. As stated in Chapter 2, it was found that the shock wave actually attenuated with distance, decreasing the shock Mach number significantly. This problem led to studies in the 1950's by Dr. Harold Mirels, who concentrated his efforts on a more accurate prediction of the available shock tube test time. His theory is based on the development of the boundary layer in the shock tube (Mirels, 1956a). The shock tube boundary layer was never included in elementary theory due to the inviscid flow assumption.

BASIC THEORY

The introduction of the boundary layer into the theoretical predictions presents some revelations. To proceed with his analysis, Mirels assumes that the boundary layer is thin compared with the shock tube diameter. The assumption is based on the premise that most shock tubes are designed for a uniform core of potential flow. The thin boundary layer forms along the walls of the shock tube behind the shock wave as shown in Figure 5. According to Mirels' theory this boundary layer emits weak expansion waves. These acoustic waves over take the shock wave, causing its attenuation (Mirels, 1956a). Previous theories for the shock wave attenuation are addressed by Mirels, but will not be discussed here.
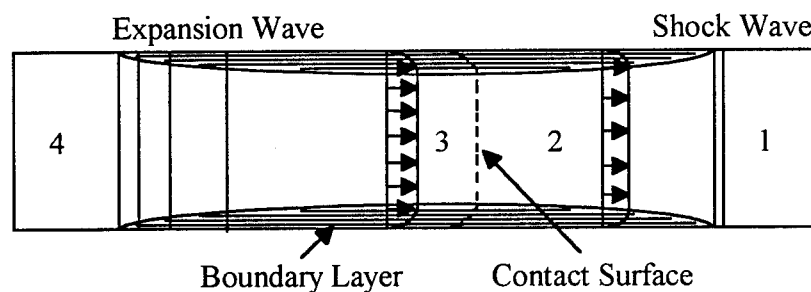
Figure 5. Shock tube flow with boundary layers (Mirels, 1956)

17

Mirels' analysis (1956a) begins with the assumption that the motion in the shock tube can be considered one-dimensional unsteady flow through a constant area. Each incremental cross-section of the tube is considered as a weak mass source which perturbs flow through the tube through the generation of pressure waves. Mirels begins his derivations with three basic equations. These equations are:

Momentum: $$\rho\left(\frac{\partial \Delta u}{\partial t} + u\frac{\partial \Delta u}{\partial x}\right) = -\frac{\partial \Delta p}{\partial x} \tag{3.1}$$

Continuity: $$\frac{\partial \Delta \rho}{\partial t} + \rho\frac{\partial \Delta u}{\partial x} + u\frac{\partial \Delta \rho}{\partial x} = m \tag{3.2}$$

Isentropy: $$\Delta p = a^2 \Delta \rho \tag{3.3}$$

Here m = m(x,t), which constitutes the rate of mass addition per unit cross-sectional area per unit x. The equations for the net perturbation at any point x, t are expressed as follows:

$$\Delta p^+ = \frac{a}{2(1+M)} \int_{-\infty}^{x} m(\xi, t - \frac{x-\xi}{a+u})d\xi \tag{3.4}$$

$$\Delta p^- = \frac{a}{2(1-M)} \int_{x}^{+\infty} m(\xi, t - \frac{x-\xi}{a-u})d\xi \tag{3.5}$$

The + superscript corresponds to a positive x-direction wave motion and the - superscript associates with a negative x-direction motion. The variable ξ is an integration variable for x.

These perturbation equations are fundamental to acoustic wave theory. They will be recalled in the following chapter to assist in basic computer code validation. The next step Mirels takes is to relate the ratio of the change in pressure over the total pressure to the normal velocity, v. A positive normal velocity yields a compression wave while a negative velocity forms an expansion wave, where the term "positive" in this case, applies to an inward normal velocity away from the wall.

For the derivation of the general shock attenuation formulas, flow in the shock tube is assumed to include ideal basic flow and small perturbations from the boundary layer. The ideal flow expansion wave is assumed to have a thickness of zero with a speed equivalent to the speed of sound in region 4, shown in Figure 5. These derivations are not relevant here, but can be found in NACA Report 1333.

At this point, Mirels' theory departs in different directions. One direction addresses wholly laminar flow in a specified region, while another solves the wholly turbulent flow region. An obvious question concerns the case where a transition from laminar to turbulent occurs within a single region of the shock tube. Although Mirels does provide a method to address this case, it is difficult to apply. In addition, acceptable methods for

determining the flow transition point have not been developed (Mirels, 1956a). Therefore, this case will not be treated here.

For the standard shock tube with a driver section, represented as region 3 in Figure 5, and a driven section, shown as region 2, four different cases are apparent. The first is the wholly laminar case, where both region 2 and region 3 contain laminar flow. The second and third cases concern a mix of flow, where one region is wholly turbulent and one is wholly laminar. The last occurs when both region 2 and region 3 are wholly turbulent. This last situation is the most common and the only case addressed in this thesis. The reasoning behind this decision is simple. The developed code from this report will first be applied to shock tubes located at Arnold Engineering and Development Center, specifically, the G-Range high performance free piston shock tunnel. The majority of these shock tubes operate in the high Reynolds number range and therefore exclusively involve wholly turbulent flow in both the driven and driver sections of the shock tubes.

As mentioned before, normal velocities occur as a result of the mass loss effects. Other effects noted by Mirels concern dissipation and heat transfer. Dissipation increases the normal velocity. Heat transfer increases

the normal velocity when passing from wall to boundary layer. The opposite situation has a decreasing effect on the normal velocity.

TURBULENT BOUNDARY LAYER

Integral methods are used to solve the turbulent boundary layer problem. This solution will be addressed in detail. Mirels (1956b) used empirical, semi-infinite flat-plate, boundary layer data applied to a moving wall to develop these solutions. The ensuing set of derivations follows the development in NACA TN 3712. For a fixed shock coordinate system, the steady flow fluid dynamic equations apply in the region bounded by the shock and the interface. Since one-dimensional shock tube theory predicts a constant pressure in this region, the boundary layer equations can be written as:

Continuity:
$$\frac{\partial \rho u}{\partial x} + \frac{\partial \rho v}{\partial y} = 0 \qquad (3.6)$$

Momentum:
$$\rho u \frac{\partial u}{\partial x} + \rho v \frac{\partial u}{\partial y} = \frac{\partial \tau}{\partial y} \qquad (3.7)$$

Energy:
$$\rho C_p (u \frac{\partial T}{\partial x} + v \frac{\partial T}{\partial y}) = -\frac{\partial q}{\partial y} + \tau \frac{\partial u}{\partial y} \qquad (3.8)$$

with the boundary conditions:

21

$$u(x,0) = u_w \qquad u(x,\infty) = u_e \qquad v(x,0) = 0$$

it is possible to find the integral form of the momentum equation. Figure 6

on the following page shows the fixed shock coordinate system used for the

derivation. Here, W from Equation 2.9 is equal to U_s, and $u_e = U_s - u_2$.

Integrating the momentum equation with respect to y from zero to δ yields:

$$\int_0^\delta \rho u \frac{\partial u}{\partial x} dy + \int_0^\delta \rho v \frac{\partial u}{\partial y} dy = -\tau_w \tag{3.9}$$

Rearranging the continuity equation provides:

$$\rho v = -\int_0^y \frac{\partial \rho u}{\partial x} dy' \tag{3.10}$$

Substitution of equation 3.10 into 3.9 gives:

$$\int_0^\delta \rho u \frac{\partial u}{\partial x} dy - \int_0^\delta \frac{\partial u}{\partial y} \left[\int_0^y \frac{\partial \rho u}{\partial x} dy' \right] dy = -\tau_w \tag{3.11}$$

Integration by parts allows for the following:

$$-u_e \int_0^\delta \frac{\partial \rho u}{\partial x} dy + \int_0^\delta (\rho u \frac{\partial u}{\partial x} + u \frac{\partial \rho u}{\partial x}) dy = -\tau_w \tag{3.12}$$

Combination of like terms and simplification confirm the integral form of the

momentum equation as:

$$\frac{\tau_w}{\rho_e u_e^2} = \frac{d}{dx} \int_0^\delta \frac{\rho u}{\rho_e u_e} (1 - \frac{u}{u_e}) dy = \frac{d\theta}{dx} \tag{3.13}$$

The term u/u_e is the average velocity. In order to continue, some

assumptions and definitions must be noted. First, the boundary layer

thickness will be noted as δ and a similarity parameter $\zeta = y/\tilde\delta$. To express

u/u_e as a function of the similarity parameter, Mirels assumes the average
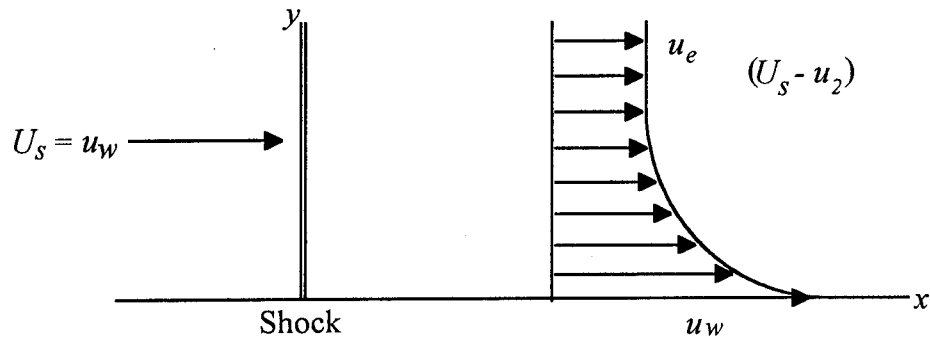
22

Figure 6. Fixed shock coordinate system

velocity will behave according to the seventh-power law, which was derived

for a turbulent boundary layer on a semi-infinite flat plate according to

Mirels. Therefore,

$$\frac{u}{u_e} = \zeta^{\frac{1}{7}} \quad \text{for} \quad 0 \le \zeta \le 1 \quad (3.14)$$

This format has provided good results for the entire range of Mach number

flows. The seventh-power law also works well for skin friction data (Mirels,

1956b). To include the moving wall profile, velocities relative to the wall

were also given a seventh-power association where:

$$\left| \frac{u - u_w}{u_e - u_w} \right| = \zeta^{\frac{1}{7}} \quad \text{for} \quad 0 \le \zeta \le 1 \quad (3.15)$$

and:

$$\left| \frac{u - u_w}{u_e - u_w} \right| = 1 \quad \text{for} \quad 1 \le \zeta \quad (3.16)$$

Other terms expressed as functions of the seventh-power law for the

necessary calculations include the following ratios with appropriate

coefficients (Mirels, 1964):

23

$$\frac{\rho_e}{\rho} = \frac{T}{T_e} = \frac{T_w}{T_e}(1 + b\zeta^{\frac{1}{7}} - c\zeta^{\frac{2}{7}}) \quad \text{for} \quad 0 \le \zeta \le 1 \qquad (3.17)$$

$$\frac{\rho_e}{\rho} = \frac{T}{T_e} = 1 \quad \text{for} \quad 1 \le \zeta \qquad (3.18)$$

Where $b = (h_r/h_w)-1$ and $c = h_r/h_w-h_{e,0}/h_w$.. Mirels combines the previous two sets of equations, Equations 3.15 to 3.18, to find the boundary layer momentum thickness:

$$\frac{\theta}{\tilde{\delta}} = 7\frac{T_e}{T_w}(1 - \frac{u_w}{u_e})[\frac{u_w}{u_e}I_6 + (1 - 2\frac{u_w}{u_e})I_7 - (1 - \frac{u_w}{u_e})I_8] \quad (3.19)$$

and the boundary layer displacement thickness:

$$\frac{\delta^*}{\tilde{\delta}} = 1 - 7\frac{T_e}{T_w}[\frac{u_w}{u_e}I_6 + (1 - \frac{u_w}{u_e})I_7] \qquad (3.20)$$

The I_N terms are defined as:

$$I_N = \int_0^1 \frac{z^N dz}{1+bz-cz^2}. \qquad (3.21)$$

The next step Mirels takes is to work toward boundary layer relationships. Assuming the wall temperature is constant, $\theta/\tilde{\delta}$ is independent of x. The integral form of the momentum equation 3.13, can be rewritten.

$$\frac{\tau_w}{\rho_e u_e^2} = \frac{\theta}{\tilde{\delta}}\frac{d\tilde{\delta}}{dx} \qquad (3.22)$$

Here, the Blasius relation is required to associate τ_w and δ which, for incompressible turbulent flow on a semi-infinite flat plate is:

$$\frac{\tau_w}{\rho_e u_e^2} = 0.0225(\frac{v_e}{u_e\tilde{\delta}})^{\frac{1}{4}} \qquad (3.23)$$

24

To solve for the boundary layer thickness, a new subscript "m" is introduced in the following equations and denotes a mean value for the appropriate variable.

$$\frac{\tau_w}{\rho_m u_e^2} = 0.0225(\frac{v_m}{u_e \tilde{\delta}})^{\frac{1}{4}} \tag{3.24}$$

$$\frac{\tau_w}{\rho_e u_e^2} = 0.0225\phi(\frac{v_e}{u_e \tilde{\delta}})^{\frac{1}{4}} \tag{3.25}$$

$$\phi = \left(\frac{\mu_m}{\mu_e}\right)^{\frac{1}{4}} \left(\frac{T_e}{T_m}\right)^{\frac{3}{4}} \tag{3.26}$$

An estimate for the mean temperature value can be found with the equation

$T_m = 0.5(T_w + T_e) + 0.22(T_r - T_e)$ (Mirels, 1956b). Multiplying a simple factor to the Equation 3.25 above gives:

$$\frac{\tau_w}{\rho_e(u_e - u_w)^2} = 0.0225\phi(\frac{v_e}{|u_e - u_w|\tilde{\delta}})^{\frac{1}{4}} \frac{u_e - u_w}{|u_e - u_w|} \tag{3.27}$$

Simplifying this equation yields:

$$\frac{\tau_w}{\rho_e u_e^2} = 0.0225\phi(1 - \frac{u_w}{u_e})\left|1 - \frac{u_w}{u_e}\right|^{\frac{3}{4}}(\frac{v_e}{u_e \tilde{\delta}})^{\frac{1}{4}} \tag{3.28}$$

Another substitution involving Equation 3.22 provides the following:

$$\frac{\theta}{\tilde{\delta}}\frac{d\tilde{\delta}}{dx} = 0.0225\phi(1 - \frac{u_w}{u_e})\left|1 - \frac{u_w}{u_e}\right|^{\frac{3}{4}}(\frac{v_e}{u_e \tilde{\delta}})^{\frac{1}{4}} \tag{3.29}$$

If T_w is considered constant, the Equation 3.29 can be integrated, giving:

$$\delta = 0.0574(\phi\frac{1 - u_w/u_e}{\theta/\tilde{\delta}})^{\frac{4}{5}}\left|1 - \frac{u_w}{u_e}\right|^{\frac{3}{5}}(\frac{v_e}{u_e x})^{\frac{1}{5}}x \tag{3.30}$$

25

In addition to these equations, some relationships dealing with enthalpy are required. The mean static enthalpy is defined by:

$$\frac{h_m}{h_{e,0}} = 0.5(\frac{h_w}{h_{e,0}} + 1) + 0.22(\frac{h_r}{h_{e,0}} - 1) \qquad (3.31)$$

where h_r is the recovery enthalpy (Mirels, 1964). The previous ratios are defined for an ideal gas as:

$$\frac{h_r}{h_{e,0}} = 1 + \frac{(W-1)^2}{ZW-1}r(0) \quad \text{and} \quad \frac{h_w}{h_{e,0}} = \frac{W(Z-W)}{ZW-1} \qquad (3.32, 3.33)$$

where

$$W = \frac{u_w}{u_{e,0}} = \frac{\rho_{e,0}}{\rho_\infty} \quad \text{and} \quad Z = \frac{\gamma+1}{\gamma-1} \quad \text{and} \quad r(0) = (Pr)^{\frac{1}{3}}$$

The r(0) term is the recovery factor. For a γ=1.4, r(0) is found to be 0.897 and for γ=1.667, r(0) = 0.875 (Mirels, 1964).

Although Mirels provides additional equations for use in many situations, only those listed here are used in the prediction code to reproduce Mirels' approach to shock wave attenuation. Integrals were performed using Simpson's Rule. All other equations were combined in a single subroutine which was then attached to an existing computer code.

26

CHAPTER IV

SHOCK TUBE PREDICTION PROGRAM

INTRODUCTION

A working computer program was the quantifying objective of this thesis. The code would be modified for each individual shock tube. Inputs would be allowed for various runs. Calculations would include shock tube characteristics and other relevant data for the test. The difference between this prediction code and those already in place would be the accurate determination of the shock Mach number, shock tube characteristics, reflected shock values, and other appropriate variables formerly estimated.

Although optimistic, expected results were not anticipated to be 100% accurate. Instead, the mass loss attenuation theory application was considered a significant step in the right direction to solving the continuing problem of the over-predicted shock velocity. With a solid foundation for more accurate prediction methods, refinements could be pursued, enhancing the effectiveness of the predictions. This would in turn allow more efficient

testing in the form of increased test precision, fewer required runs, and better computational methods. The indirect advantage is monetary savings, which is a welcomed result in any field of endeavor.

THE PROGRAM DESCRIPTION

The basic code used for this Fortran computer program was adapted from an existing prediction code for the free piston shock tunnel located at AEDC. The original code was applied to the free piston shock tunnel in 1989 (Maus, 1994). Despite its origins, the computer algorithm can be applied to any turbulent boundary layer shock tube.

This program operates in increments of position within increments of time in a Lagrangian format. A tube is separated into the two basic shock tube sections: the driver section and the driven section. Each has its own set of initial conditions corresponding to the appropriate shock tube dimensions and setup. Each shock tube section is divided into a specified number of zones which remains fixed for a given run. These zones contain a initial amount of mass, determined by the volume of the tube and type of gas in the tube. The mass is considered to be concentrated in two halves at the center

of each respective volumetric dividing line. Figure 7 depicts some of the notation and concepts of the code methodology. Newtonian dynamics govern the movement of the mass particles while the basic theory solves variables such as pressure, volume, and energy. For each cycle, increments of time and distance are added to advance the shock tube system. The program is set up to terminate at the end of a selected number of cycles or when the shock reaches the end of the tube, whichever occurs first. The program can be modified to terminate for other events as well or continue into the reflected shock regime, although attenuation calculations would require some modifications.

Within a time step, the program is governed by five basic equations. The first three involve Newton's second law. Velocity and displacement are determined for each mass point by these three equations:

$$\frac{dU}{dt} = (PQ_{J-\frac{1}{2}} - PQ_{J+\frac{1}{2}} - DPF)\frac{A_J^N}{m_J} \qquad (4.1)$$

$$U_J^{N+1} = U_J^N + \overline{\frac{dU}{dt}}dt \qquad (4.2)$$

$$X_J^{N+1} = X_J^N + U_J^{N+1} dt^N \qquad (4.3)$$

The term PQ is a pressure term where P is the pressure and Q is a dissipation factor. Q is proportional to the square of the local velocity gradient whose
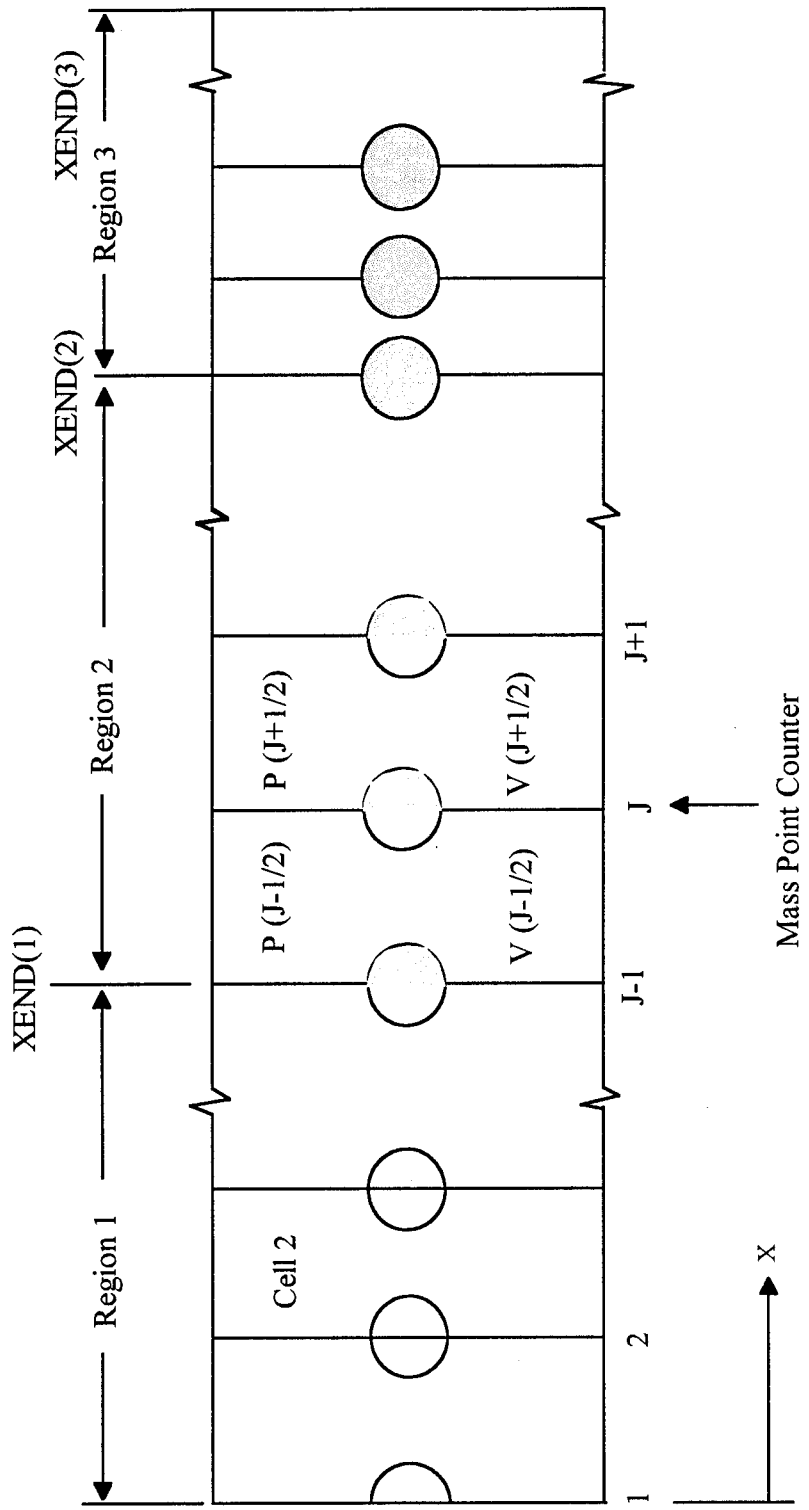
Figure 7. Mass points, cells and regions (Maus, 1991)

value is only significant near the shock wave. DPF represents a drop in pressure due to friction forces on the mass point (Maus, 1991).

The next two equations, energy and equation of state, solve the change in energy and the pressure. The equation forms used in the program are:

$$dE = dQ_w - PQdV \qquad (4.4)$$

$$P = f(E, V) = \frac{(\gamma-1)E}{V} \qquad (4.5)$$

The term dQ_w is found using Newton's law of cooling. With these two variables known, the rest of the thermodynamic variables can be determined.

The mass loss subroutine, labeled SINK, contains the equations for the attenuation algorithm which were noted in Chapter 3. The three necessary integral terms are solved using Simpson's Rule. The equations for the boundary layer momentum thickness, $\frac{\theta}{\delta}$ (Equation 3.19), and $\frac{\delta^*}{\delta}$ (Equation 3.20) the displacement thickness, help provide the following relationships.

$$\delta \propto \frac{x}{Re_x^{0.2}} \qquad (4.6)$$

This equation is derived from Equation 3.30. The normal velocity is found to be,

$$v = U_e \frac{d\delta^*}{dx} \qquad (4.7)$$

The mass flow into the boundary layer is,

$$\dot{m} = \rho_e U_e \frac{d\delta^*}{dx} P\Delta x \qquad (4.8)$$

31

This mass flow term represents the net change in mass leaving the potential flow and entering the boundary layer, causing the perturbations. Since this mass flow term comes from one unit of mass it must be split in half. Recall that each mass point is separated into two equal parts, residing in adjacent volume cells. Two different half mass terms are used to account for the total mass in the cell. To summarize, a mass flow into the boundary layer was calculated. The mass traveling into the boundary layer was subtracted from the mass in the potential flow, giving a new half mass term. This new half mass term is carried through on the next iteration and used to solve the next increment of shock tube characteristics.

METHOD VALIDATION

In order to determine whether the computer code algorithm was accurate, acoustic theory was applied and solutions were compared. The code was simplified to act on a single region tube. The initial state variables were constant throughout the tube. At some time, t, the mass of a cell in the center of the tube was altered and the resulting motion was examined and compared with an exact solution from acoustic wave theory.

The computer code was modified by the author to produce the acoustic results. The following calculations and figures were provided for comparison (Maus, 1994). The equation for the propagation of an acoustic wave is:

$$\Delta p^+(x, t) = \frac{a}{2} \int_{-\infty}^{x} m(\xi, t - \frac{x-\xi}{a}) d\xi \qquad (4.1)$$

where, $m(x,t) = M_a$, for $x_1 < x < x_2$ and $t > 0$. Equation 4.1 is another form of Equation 3.4 from Mirels' report (Mirels, 1956a). The m term is the rate of mass addition per unit cross sectional area per unit length. Figure 8 displays the mass source region and a random point, x, for an acoustic wave propagation tube. Solutions for given intervals of t and a fixed field point, x, are as follows:

$$0 < t < \frac{x-x_2}{a} \qquad \Delta p^+(x, t) = 0$$

$$\frac{x-x_2}{a} < t < \frac{x-x_1}{a} \qquad \Delta p^+(x, t) = \frac{a}{2} M_a(x_2 - (x - at))$$

$$t > \frac{x-x_1}{a} \qquad \Delta p^+(x, t) = \frac{a}{2} M_a(x_2 - x_1)$$
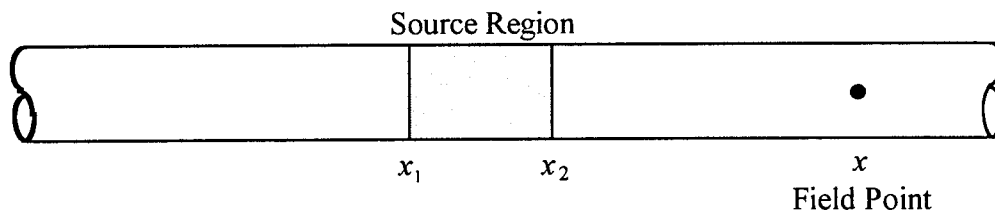
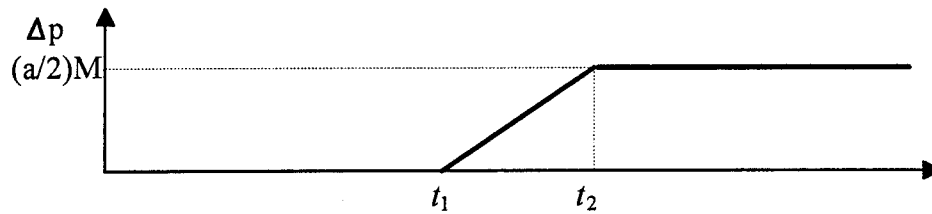Figure 8. Acoustic wave tube diagram (Maus, 1994)

Figure 9. Fixed field point graph (Maus, 1994)

Figure 9 is a graphical summary of the set of solutions for the fixed field point. Here, $t_1 = (x - x_2)/a$, and $t_2 = (x - x_1)/a$. The next set of solutions are given over the interval x for a fixed time, t. Figure 10 is the graphical representation for the fixed time case.

$$x > x_2 + at \qquad \Delta p = 0$$

$$x_1 + at < x < x_2 + at \qquad \Delta p = \tfrac{a}{2} M_a(x_2 - (x - at))$$

$$x < x_1 + at \qquad \Delta p = \tfrac{a}{2} M_a(x_2 - x_1)$$

With this ground work, numbers were substituted for variables in the exact solution and the computer code. The following variables were set at: length
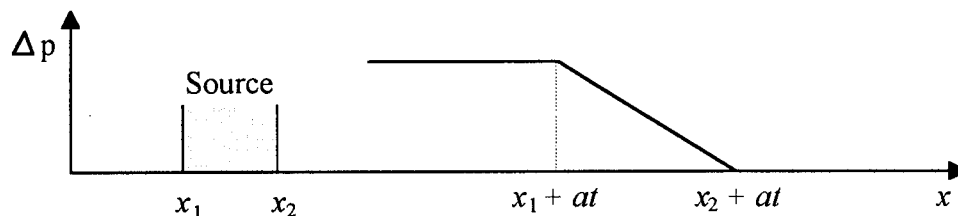
Figure 10. Fixed time graph (Maus, 1994)

34

= 1000 cm, Δx_0 = 5 cm, $x_2 - x_1$ = 25 cm, diam = 8 cm, A = 50.26 cm^2, F = 0.01 (reduction in mass per step), a = 347 m/sec, and M_a is found to equal 0.07958 gm/sec/cm^3. These numbers yield: Δp = 0.03451 bar and p = 1.0345 bar.

Figures 11 and 12 show the program generated results along with the exact solutions at t = 2 and 4 msec, respectively. Figure 11 shows no difference between the two methods. Figure 12 indicates a slight difference. This difference increases with time, but remains within the bounds of acceptable error. Therefore, the conclusion can be drawn that the program models acoustic propagations accurately indicating that it should model the mass loss algorithm adequately.

The computer code has been shown to match the acoustic theory well. However, this evidence is not conclusive. In order to examine the program effectiveness, a plot of the pressure distribution is necessary. The plot should resemble the theoretical plot in Figure 4. Figure 13 shows an acceptable match between the theory and the computer results. Classical theory results are also shown in Figure 13.
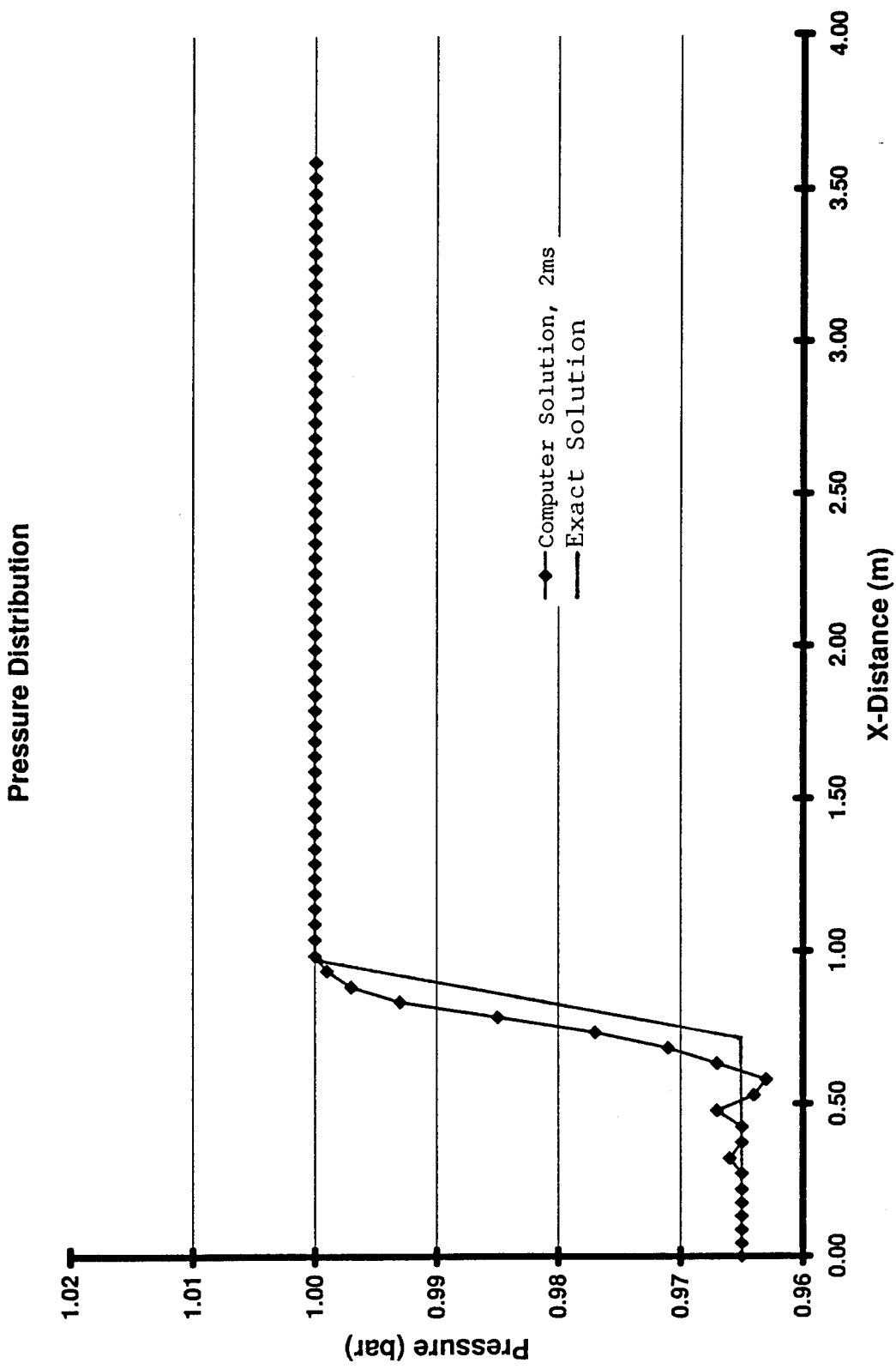
Pressure Distribution

Figure 11. Acoustic wave propagation for t = 2 ms (Maus, 1994)

Pressure Distribution
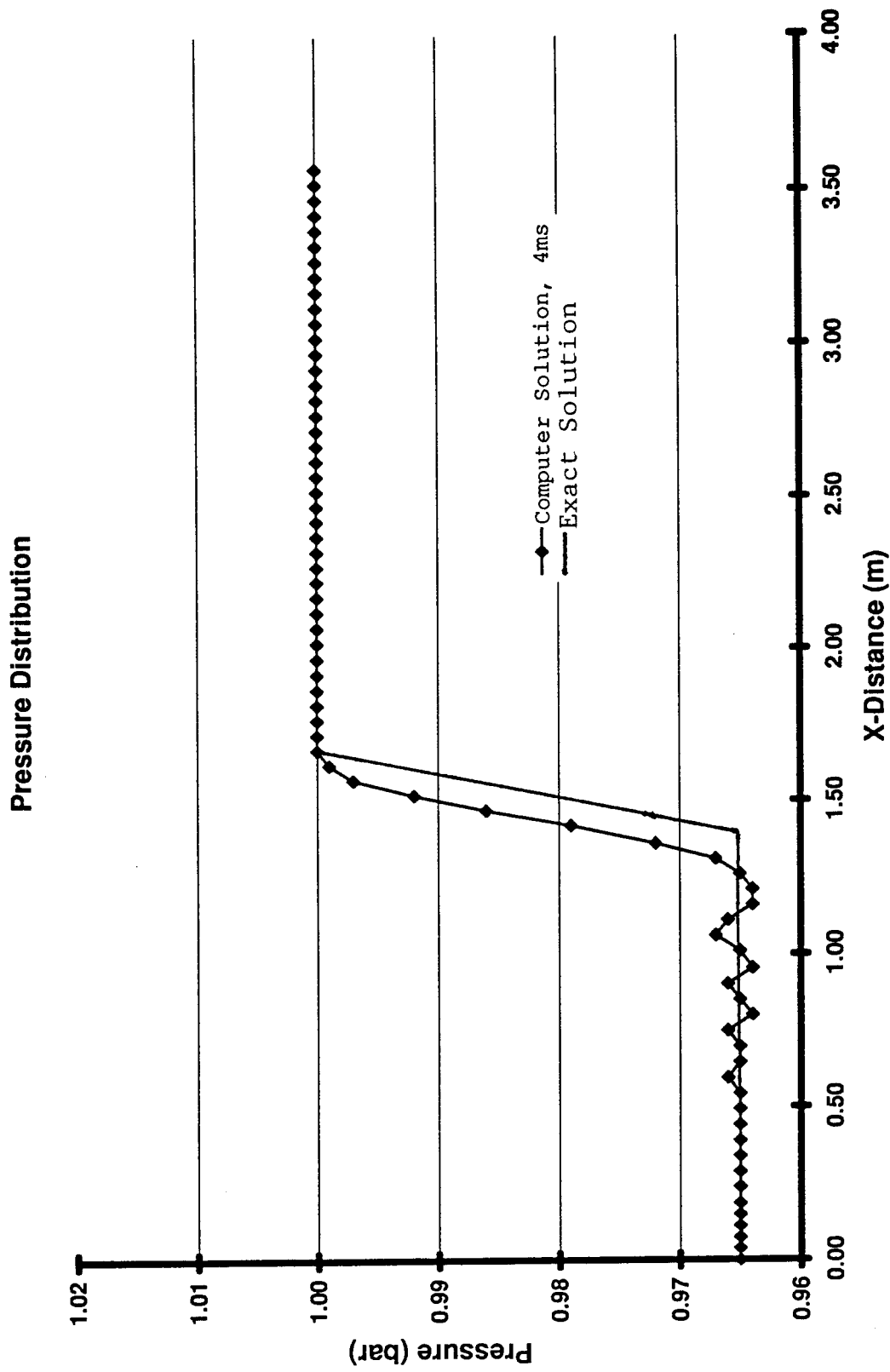
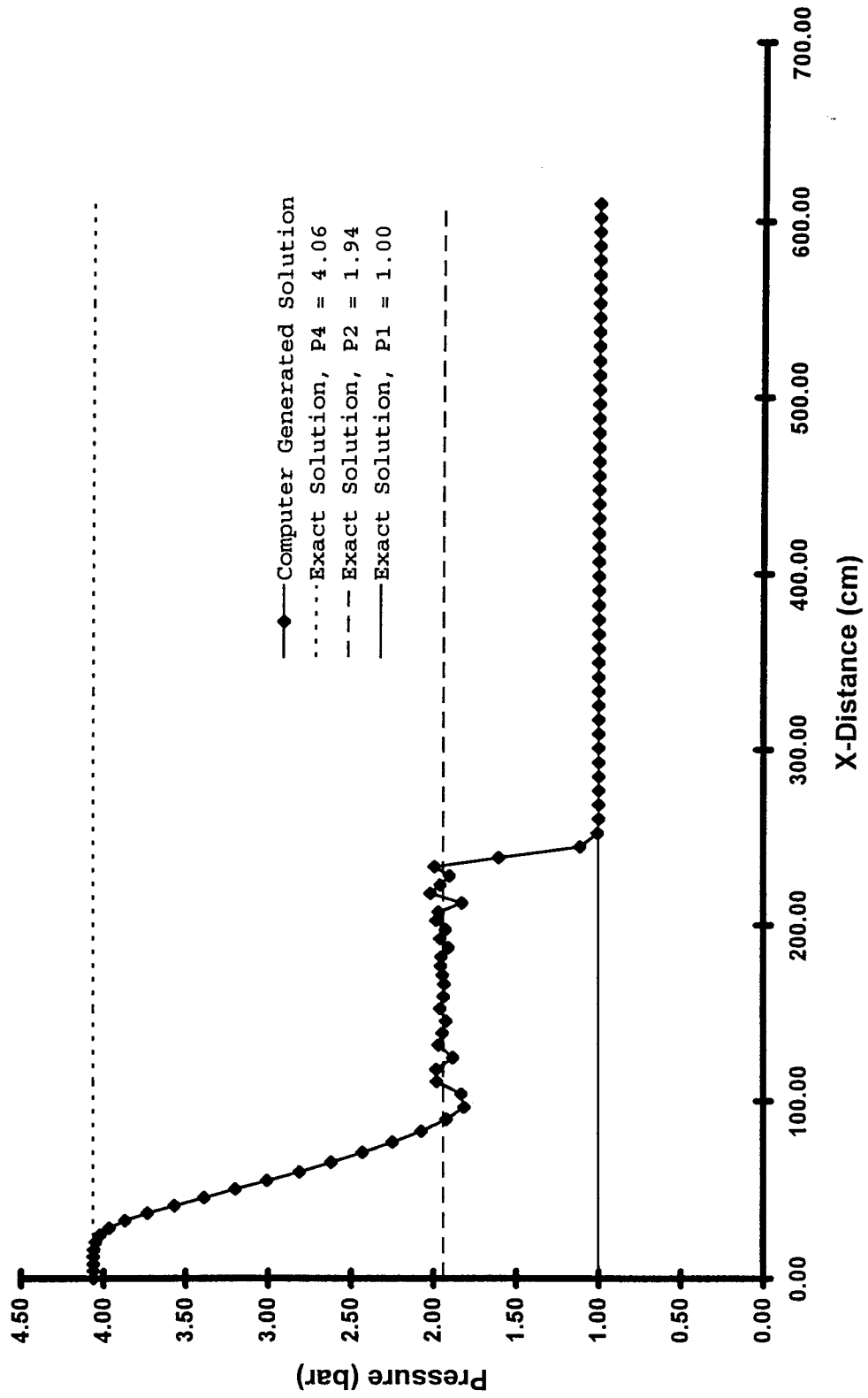Figure 12. Acoustic wave propagation for t = 4 ms (Maus, 1994)

Figure 13. Pressure distribution from computer code for P4/P1=4.061

CHAPTER V

RESULTS

INTRODUCTION

Results from the computer code were easy to produce. Difficulty came when the search was begun for reliable shock tube data which included the shock tube initial settings, dimensions, and a measured characteristics at known x locations. Additionally, comparisons were made within a single run, comparing the mass loss algorithm with the classical approach and examining the attenuation through graphs.

Two shock tube configurations were selected. The first set of cases addresses the four runs used by Mirels in his validation (Mirels, 1956a). Here, the shock Mach number range is approximately 1.3 to 1.8. The second set involves data from a research shock tube for diagnostic development at Arnold Engineering and Development Center. The Mach number for this set of data is approximately 4.0. The results varied from excellent to fair within

each case. Adjustments to the code were made as a consequence of initial figures.

RESULTS

The attenuated/ideal pressure ratio, $P_{2,d}/P_2$, has been plotted by Mirels for four separate shock tube runs. The ratio represents an excellent indicator of the shock wave attenuation in a shock tube. For this reason, the data was used to compare with results from the computer code. The code results were compared with Mirels' graphs to ensure conformity. The computer code graphs are included here for each of the four pressure ratios. In the following figures, as in Mirels' graphs, $P_{2,d}$ represents the calculated pressure immediately behind the shock wave using the mass loss equations. In order to maintain uniformity, ten pressure terms behind the shock were averaged to find $P_{2,d}$. P_2 is the pressure behind the shock, calculated by the computer code without the mass loss corrections. It was also determined by the average of ten pressure terms immediately behind the shock wave. Figures 14 through 17 show the results for the four initial pressure ratios. The squares indicate the experimental measured points from Mirels' source data.
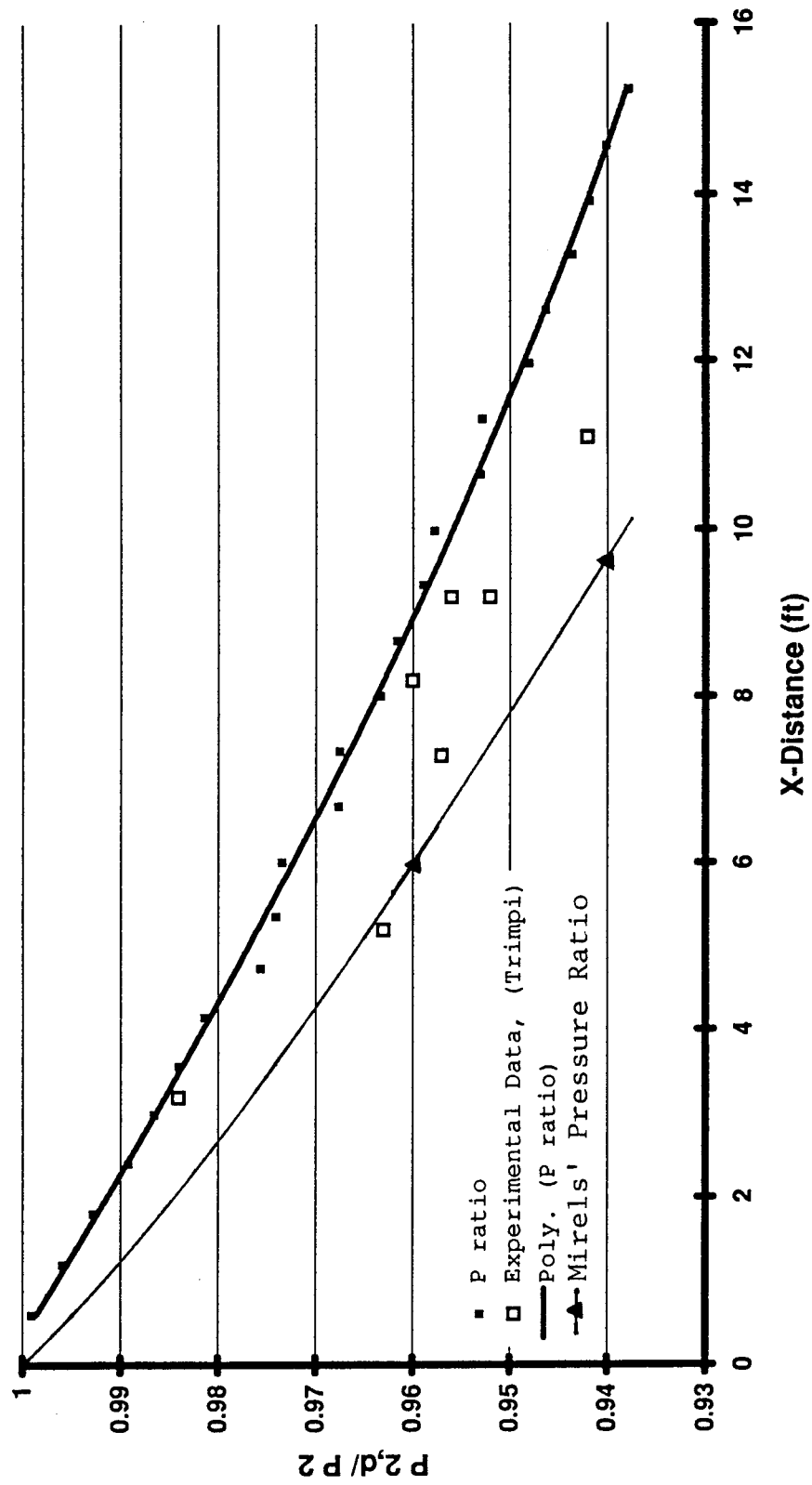
P4/P1 = 4.061

Figure 14. Comparison graph generated from computer program for M=1.313

Figure 15. Comparison graph generated from computer program for M=1.406
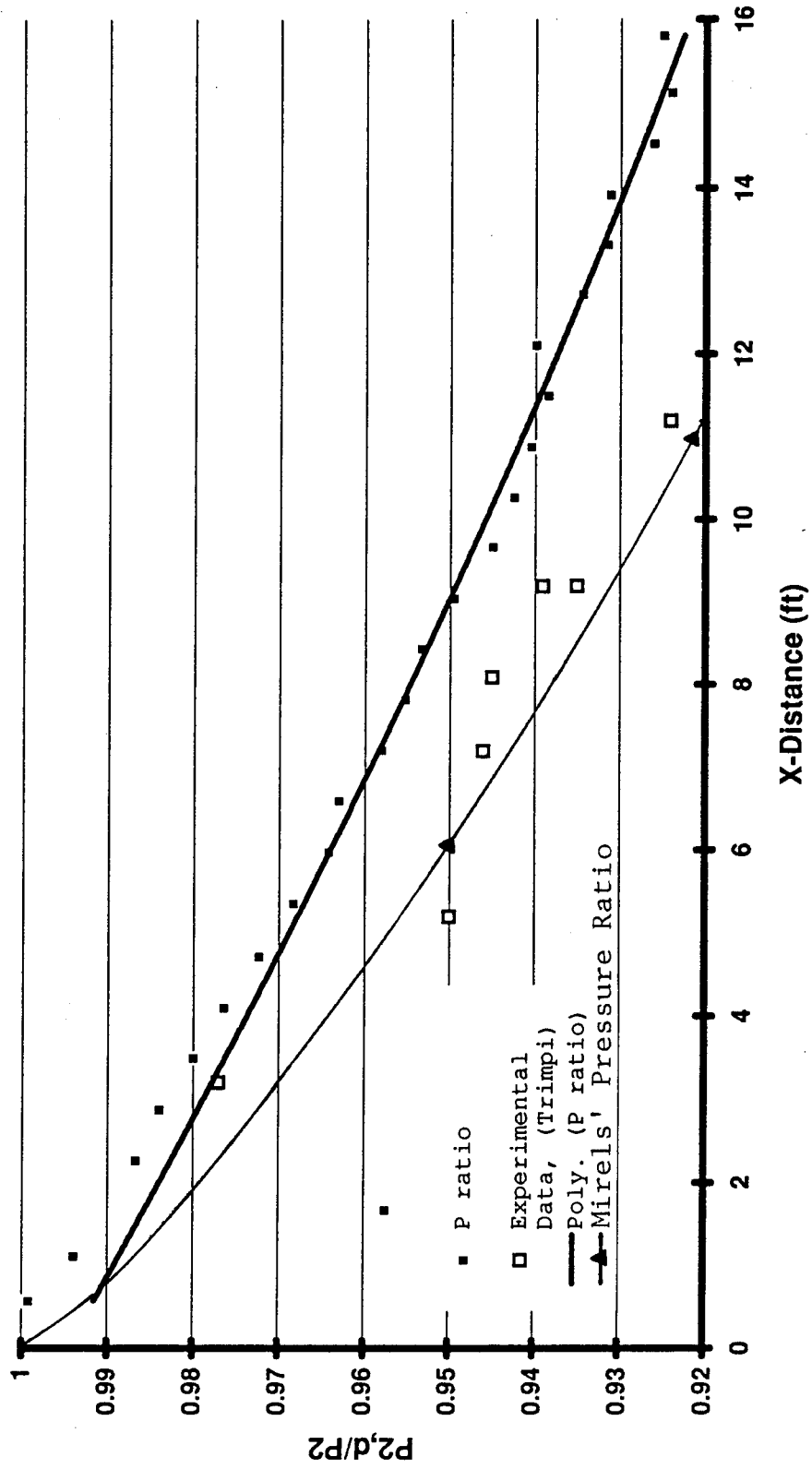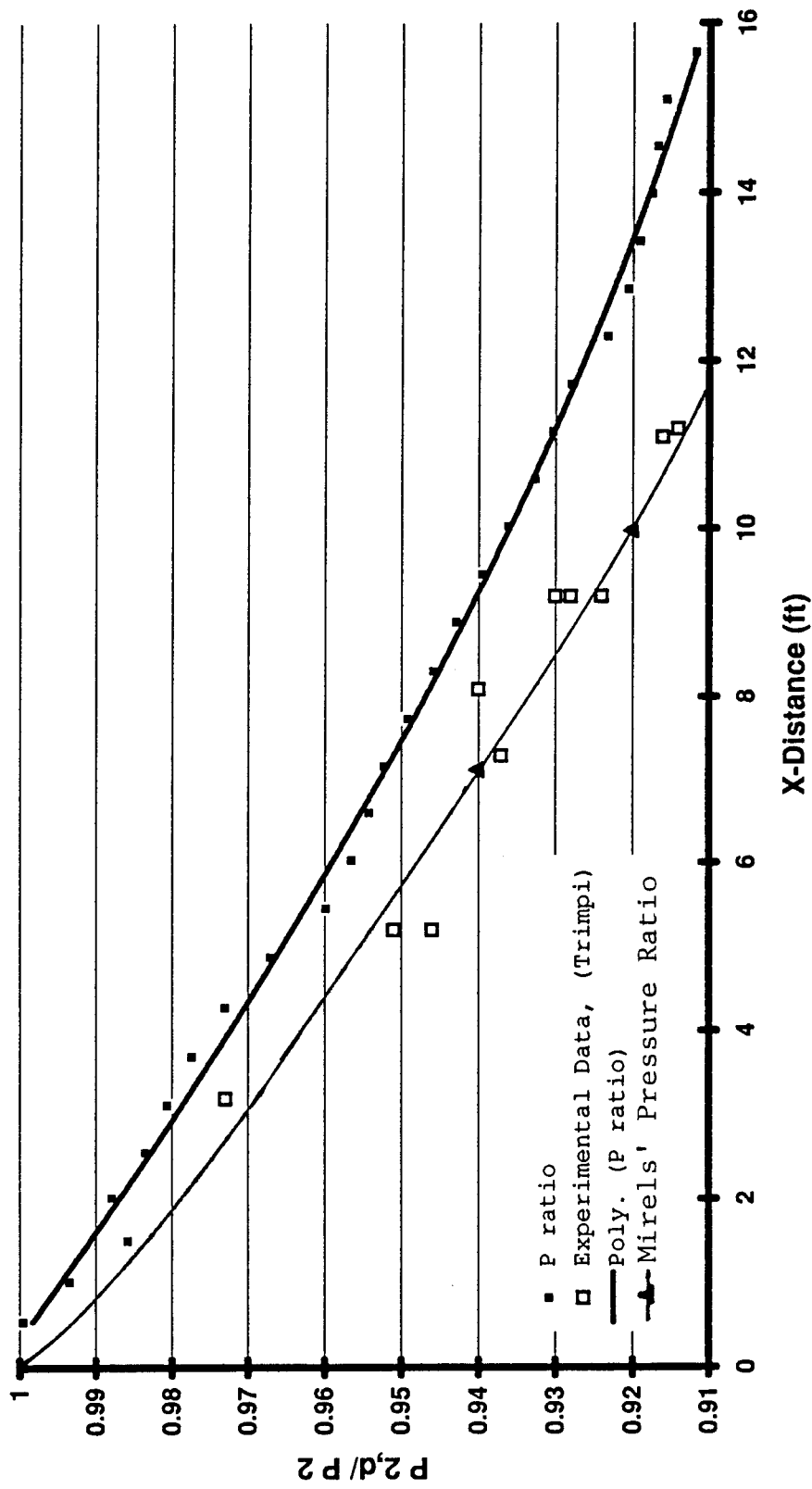
Figure 16. Comparison graph generated from computer program for M=1.470
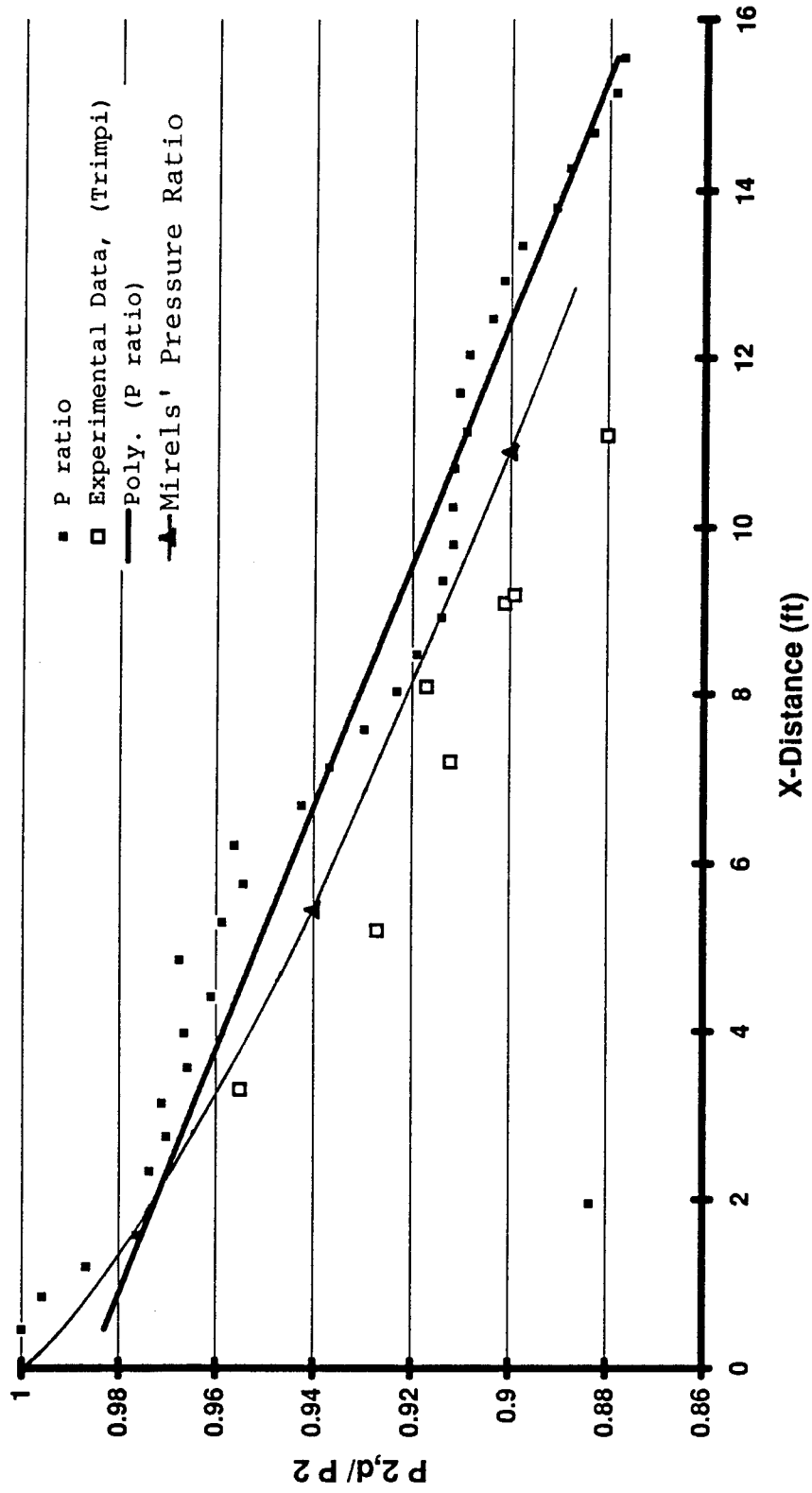
P4/P1 = 17.915

Figure 17. Comparison graph generated from computer program for M=1.718

44

P ratio is the calculated computer results. The line through the P ratio points is a polynomial regression. The line containing the triangular flags shows Mirels' calculated results (Mirels, 1956a). The Mach numbers are averaged over the length of the tube and are calculated with the mass loss subroutine. Although the computer program solutions are slightly erratic, they are acceptable. The trend for all four graphs is an overestimated pressure ratio, indicating an underestimated attenuation. However, a difference between the results of the mass loss algorithm and the classical solutions is evident. Uncorrected Mach numbers calculated by the computer program for the four previous cases were: $M = 1.34$, 1.45, 1.52, and 1.78, respectively.

To demonstrate the attenuation phenomenon, plots were generated comparing the shock wave locations, with respect to time, for program runs with and without the mass loss subroutine. Figure 18 is one of those plots, showing the mass loss data as diamonds (upper line) and the classical data as a vertical dash (lower line). This data is based on inputs and characteristics from the diagnostic development shock tube at AEDC. This shock tube uses a Helium driver and a Nitrogen driven section. For the case in Figure 18, the driver pressure, P_4, is 860 psi. The driven section pressure, P_1, is 1.47 psi.
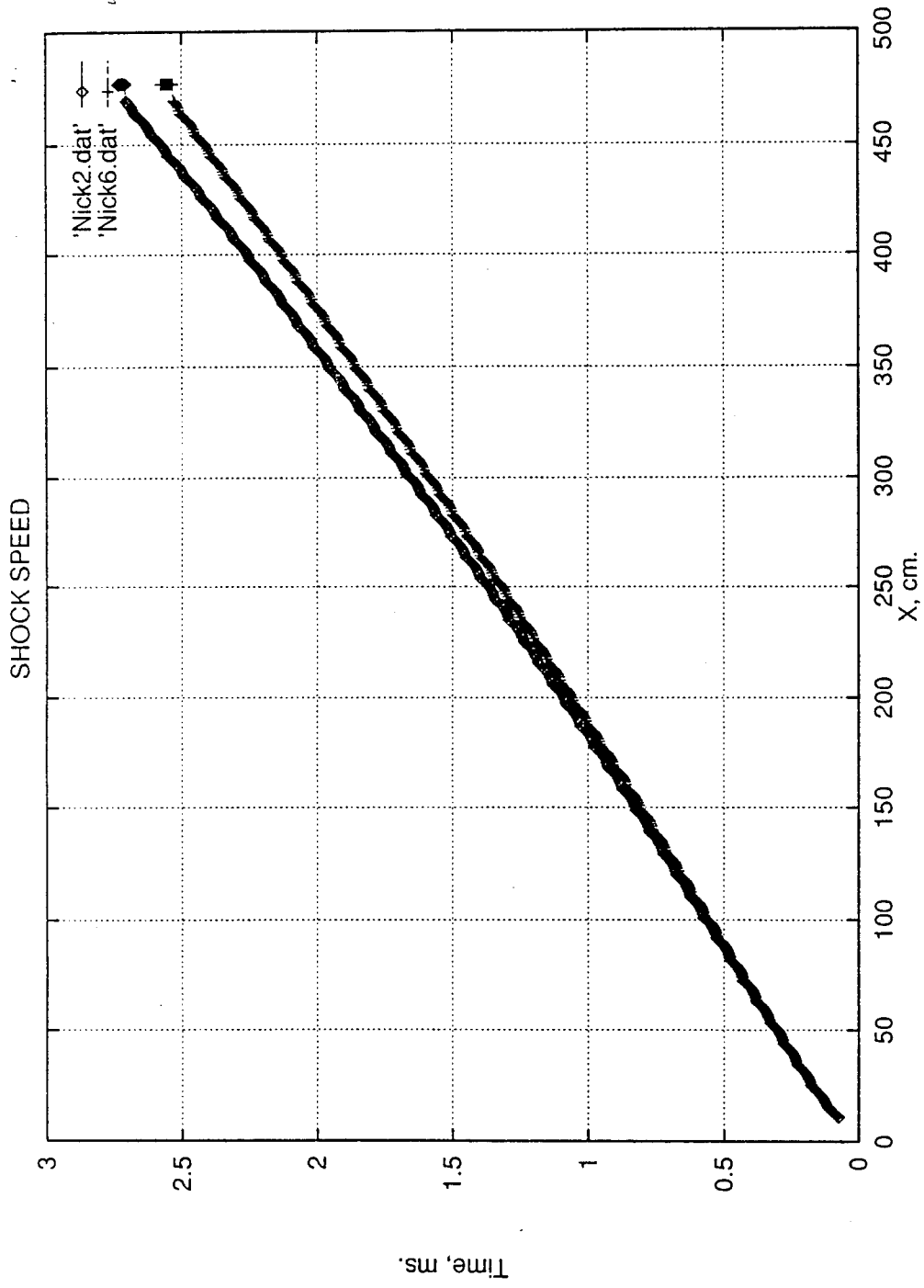
Figure 18. Shock wave attenuation comparison graph

46

The mass loss line in Figure 18 obviously slows with time and distance. Plots for other cases, including Mirels', show similar trends. The undulations in the plots illustrate the difficulty in determining the location of a computationally captured shock wave.

The next set of graphs deal with the diagnostic development shock tube at AEDC. Three cases are examined and labeled: A, B, and C. All three cases have a driver pressure (P_4) of 860 psi. The driven pressures (P_1) for the runs are: 76 torr (1.47 psi), 50 torr (0.967 psi), and 115 torr (2.22 psi), respectively. Each case was computed with and without the mass loss subroutine. Both shock speed calculations are plotted in the following figures, as are the measured shock speed data (Smith, 1994).

Figure 19 shows Case A. Excellent agreement is observed between the mass loss prediction values and the measured values. Computer results without the mass loss subroutine differ by almost 30%. Unfortunately, this case cannot stand alone and Figure 20 displays over-predicted results for Case B. Case B contains the largest initial pressure ratio of the three runs. It could therefore be assumed that Case C, having the lowest pressure ratio, will have under-predicted results. Figure 21 proves this conclusion is

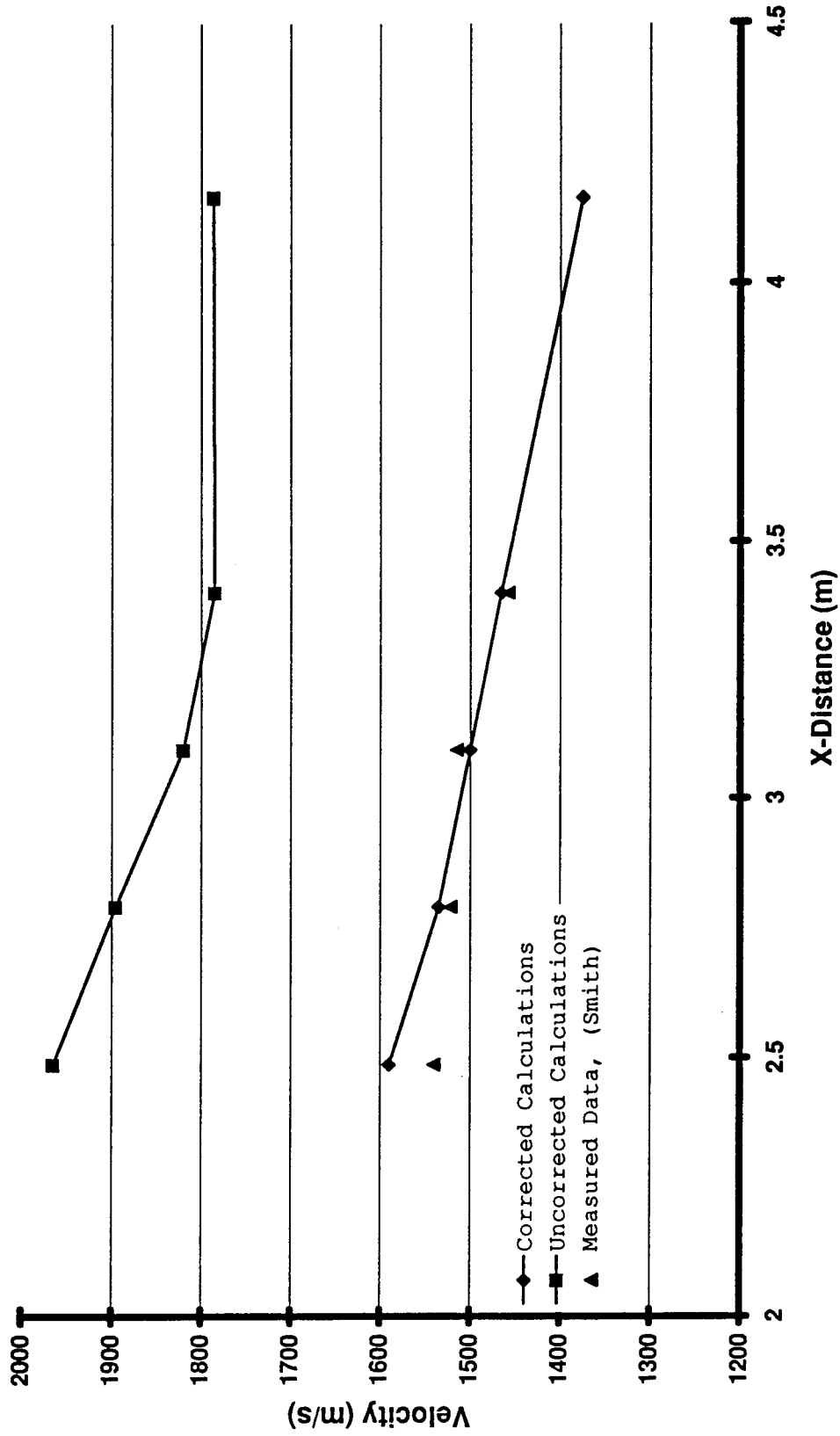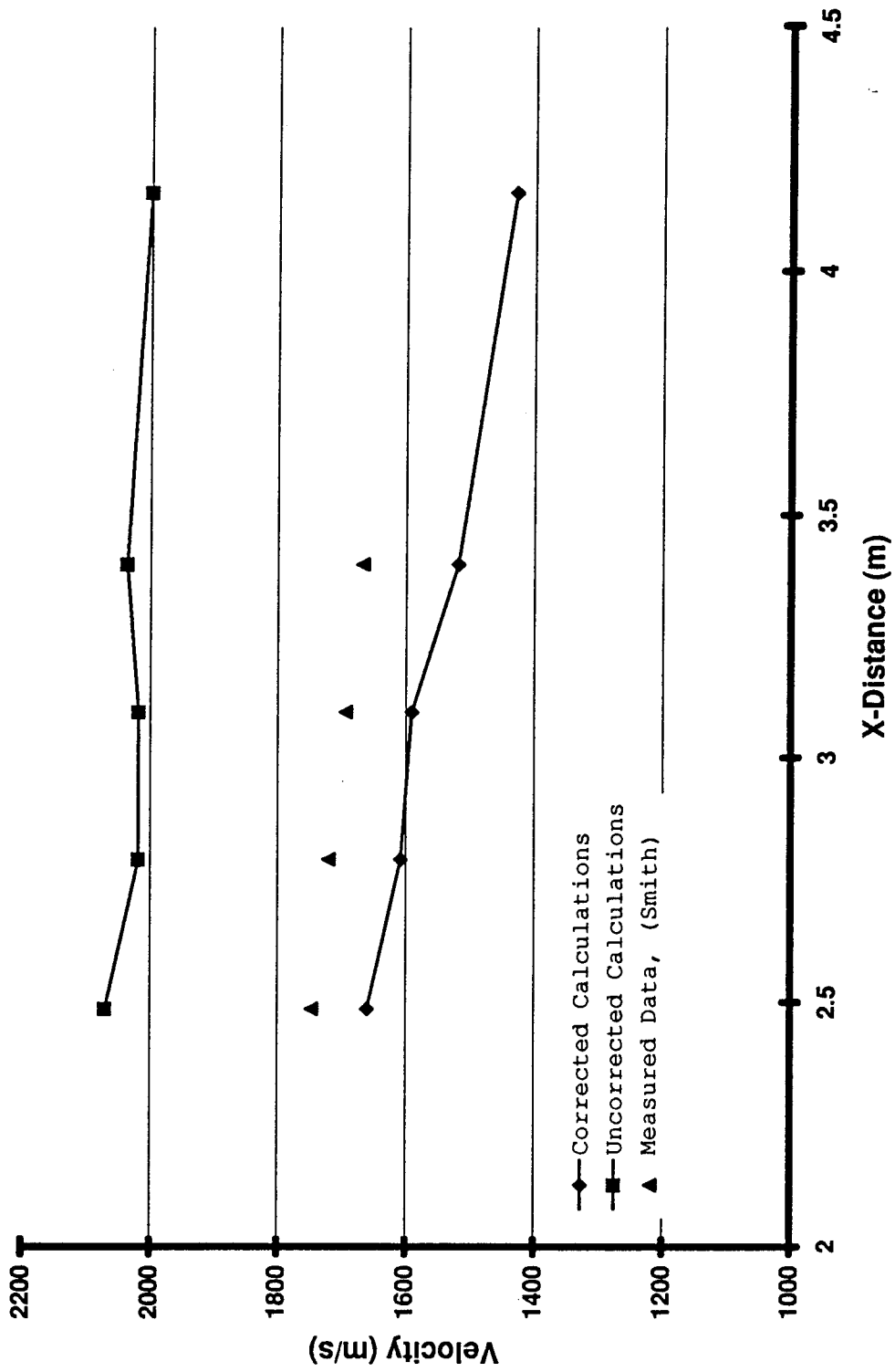Figure 19. Diagnostic development shock tube shock wave velocity: Case A

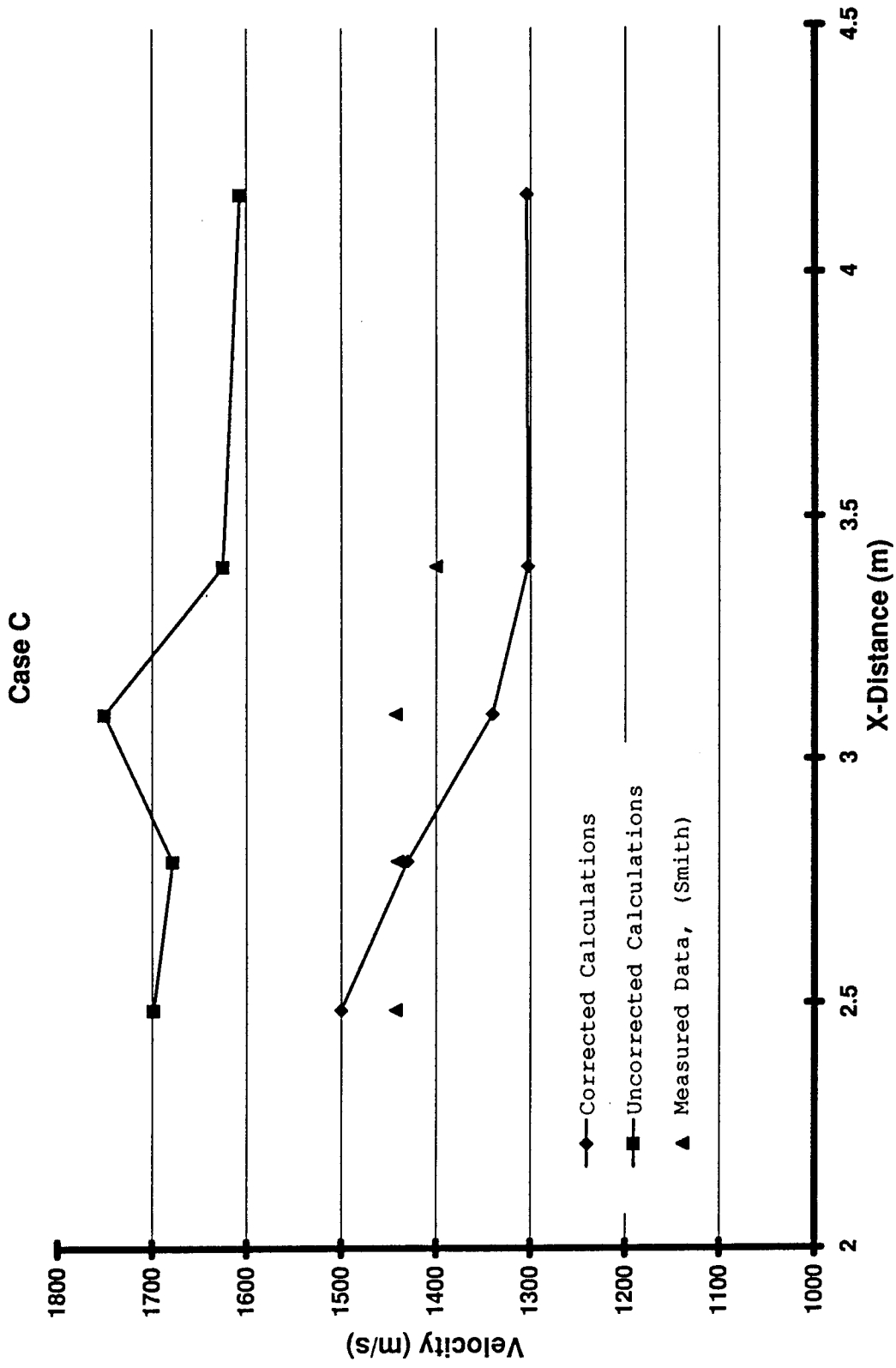Figure 20. Diagnostic development shock tube shock wave velocity: Case B

Figure 21. Diagnostic development shock tube shock wave velocity: Case C

incorrect although the initial tendency favored the hypothesis.

One last comment concerns a comparison between mass loss corrections and heat/friction corrects. The first case from Mirels, $P_4/P_1 = 4.061$, was run in four different configurations (Mirels, 1956a). The first run included mass loss and heating and friction corrections. The average shock Mach number for this run was calculated at 1.31. When only mass loss corrections were considered, the new Mach number was 1.33. Conversely, heating and friction corrections alone yielded $M_s = 1.34$. The last run with no corrections showed a Mach number of 1.36. Therefore, the mass loss equations have a large affect relative to the heating and friction corrections.

CHAPTER VI

CONCLUSION

<u>BENEFIT</u>

The difficulties in operating shock tubes in an efficient manner have been made evident in this thesis. Many problems arise in correctly predicting shock tube performance in order to utilize its testing versatility. These problems include burst diaphragm interactions, materials limits, and shock wave attenuation, to name a few. These problems, however, are only general in nature and involve many sub-problems which contribute to the overall understanding of shock tube characteristics.

In order to solve the attenuation problem, several areas must be addressed. These areas include, but are not limited to: shock wave wall friction, heat transfer, real gas effects, and the subject of this thesis, the viscous wall boundary layer interaction produced by passage of the shock wave. This boundary layer interaction introduces the mass loss phenomenon

to both turbulent and laminar flow. In turn, the mass loss affects the shock wave, the contact surface, and the expansion wave.

This thesis has focused on a specific portion of the larger problem; the effect of the mass loss on the shock wave for turbulent flow in a shock tube. This work has led to some promising results throughout the range of Mach numbers and including different shock tube configurations. The computer code produced in the process of this study can be applied readily to any shock tube. The result will improve shock tube characteristic predictions and allow for more efficient testing and a better understanding of shock tube performance.

RECOMMENDATIONS

The major recommendations consist of those applications not addressed completely in this study. The mass loss equations were applied only to the boundary layer between the shock wave and the contact surface because of the fixed shock, steady state equations. An extension would involve analyzing the mass loss contribution by the boundary layer in the expansion region and the interface region.

Friction and heat corrections were estimated here to provide approximate results. A detailed analysis of the friction between the moving shock wave and the shock tube wall could be initiated. Because of the high temperatures produced by shock tubes, heating corrections between the internal gas and the shock tube wall should be examined. The next step would involve a complete analysis of the real gas effects in a shock tube. Depending on the Mach number, real gas effects could account for a secondary portion of the prediction error.

Lastly, the laminar boundary layer could be examined. Mirels developed a separate set of equations to solve this regime. For this thesis, these equations were dismissed from an analysis standpoint, due to time constraints. Laminar flows may appear in a large quantity of shock tubes, since shock tubes can operate in the lower Mach number regions. Also, a transition analysis may prove important, since a large difficulty exists in actually determining when the boundary layer transition occurs inside the shock tube.

These recommendations are just a few suggestions where improvements can be made. Additional work can be continued where this

thesis left off. The results found here have been impressive. The author feels that a significant step has been made toward the goal of better efficiency for predictions in shock tube testing.

BIBLIOGRAPHY

56

BIBLIOGRAPHY

Anderson, John D., Jr. Modern Compressible Flow With Historical Perspective. 2nd ed. New York: McGraw-Hill, 1990. 207-214.

Campbell, John W. "Enhanced Vision Systems." Thesis University of Tennessee Space Institute 1994.

Glass, I. I. "Appraisal of UTIAS Implosion-Driven Hypervelocity Launchers and Shock Tubes." Progress In Aerospace Sciences. Ed. D. Kuchemann. vol. 13. Oxford: Pergamon Press, 1972.

Glass, I. I. "Beyond Three Decades of Continuous Research at UTIAS on Shock Tubes and Waves." AFOSR-TR-81-0783 University of Toronto, 1981. 1-12.

Gottlieb, J. J., and Glass, I. I. "Recent Developments In Sonic-Boom Simulation Using Shock Tubes." Recent Developments In Shock Tube Research: Proceedings of the Ninth International Shock Tube Symposium. Stanford University, 1973.

Maus, J. R. "A Mathematical Model for the G-Range Impulse Facility." AEDC-TMR-91-V10 October, 1991.

Maus, J. R., Laster, M. L., and Hornung, H. G. "The G-Range Impulse Facility - A High Performance Free-Piston Shock Tunnel." AIAA Paper 92-3946 July, 1992.

Maus, J. R. Personal communication between May and December, 1994.

Mirels, H. "Attenuation In a Shock Tube Due to Unsteady-Boundary-Layer Action." NACA Report 1333 April, 1956 a.

Mirels, H. "Boundary Layer Behind Shock or Thin Expansion Wave Moving Into Stationary Fluid." NACA TN 3712 May, 1956 b.

Mirels, H. "Shock Tube Test Time Limitation Due to Turbulent-Wall Boundary Layer." AIAA J. 2, 84 1964.

Smith, M. S. Personal communication concerning the diagnostic development shock tube at AEDC August, 1994.

Trimpi, R. L., and Cohen, N. B. "A Theory For Predicting the Flow of Real Gases in Shock Tubes With Experimental Verification." NACA TN 3375 March, 1955.

Wright, J. K. Shock Tubes. New York: John Wiley & Sons, Inc., 1961. 1-2.

VITA

Nick Roger McKenzie was born in Fremont, California. He attended Ponderosa High School in Shingle Springs, California. After graduating in 1988, he was admitted to the United States Air Force Academy where he majored in Aeronautical Engineering. Lt. McKenzie graduated from the Air Force Academy with a Bachelor of Science degree in 1992. He married Melissa Anne Eagan that same year and was assigned to the 33rd Flying Training Squadron at Reese AFB, Texas, for Undergraduate Pilot Training. In 1993, Lt. McKenzie was assigned to the 52nd Flying Training Squadron to complete flying training in the T-1 Jayhawk. After graduating from pilot training in 1993, Lt McKenzie was awarded an AFIT scholarship to the University of Tennessee Space Institute.